

JOURNAL OF GLACIOLOGY



CAMBRIDGE
UNIVERSITY PRESS

THIS MANUSCRIPT HAS BEEN SUBMITTED TO THE JOURNAL OF GLACIOLOGY AND HAS NOT BEEN PEER-REVIEWED.

Mass loss of the Antarctic ice sheet until the year 3000 under a sustained late-21st-century climate

Journal:	<i>Journal of Glaciology</i>
Manuscript ID	JOG-21-0083.R2
Manuscript Type:	Article
Date Submitted by the Author:	n/a
Complete List of Authors:	Chambers, Christopher; Hokkaido University Institute of Low Temperature Science, Glaciology Greve, Ralf; Hokkaido University, Institute of Low Temperature Science; Hokkaido University Arctic Research Center Obase, Takashi; The University of Tokyo Atmosphere and Ocean Research Institute Saito, Fuyuki; Japan Agency for Marine-Earth Science and Technology Yokohama Institute for Earth Sciences, RIGC Abe-Ouchi, Ayako; The University of Tokyo Atmosphere and Ocean Research Institute
Keywords:	Ice-sheet modelling, Antarctic glaciology, Ice and climate
Abstract:	Ice-sheet simulations of Antarctica extending to the year 3000 are analysed to investigate the long-term impacts of 21st century warming. Climate projections are used as forcing until 2100 and afterwards no climate trend is applied. Fourteen experiments are for the "unabated warming" pathway, and three are for the "reduced emissions" pathway.

	<p>For the unabated warming path simulations, West Antarctica suffers a much more severe ice loss than East Antarctica. In these cases, the mass loss amounts to an ensemble average of 3.5 m sea-level equivalent by the year 3000 and 5.3 m for the most sensitive experiment. Four phases of mass loss occur during the collapse of the West Antarctic Ice Sheet. For the reduced emissions pathway, the mean mass loss is 0.24 m sea-level equivalent. By demonstrating that the consequences of the 21st century unabated warming path forcing are large and long-term, the results present a different perspective to ISMIP6 (Ice Sheet Model Intercomparison Project for CMIP6). Extended ABUMIP (Antarctic BUttrressing Model Intercomparison Project) simulations, assuming sudden and sustained ice-shelf collapse, with and without bedrock rebound corroborate a negative feedback for ice loss found in previous studies, where bedrock rebound acts to slow the rate of ice loss.</p>

SCHOLARONE™
Manuscripts

Mass loss of the Antarctic ice sheet until the year 3000 under a sustained late-21st-century climate

Christopher CHAMBERS,^{1*} Ralf GREVE,^{1,2} Takashi OBASE,³ Fuyuki SAITO,⁴

Ayako ABE-OUCHI³

¹*Institute of Low Temperature Science, Hokkaido University, Sapporo, Japan*

²*Arctic Research Center, Hokkaido University, Sapporo, Japan*

³*Atmosphere and Ocean Research Institute, The University of Tokyo, Kashiwa, Japan*

⁴*Japan Agency for Marine-Earth Science and Technology, Yokohama, Japan*

Correspondence: Christopher Chambers <youstormorg@gmail.com>

ABSTRACT. Ice-sheet simulations of Antarctica extending to the year 3000 are analysed to investigate the long-term impacts of 21st century warming. Climate projections are used as forcing until 2100 and afterwards no climate trend is applied. Fourteen experiments are for the “unabated warming” pathway, and three are for the “reduced emissions” pathway. For the unabated warming path simulations, West Antarctica suffers a much more severe ice loss than East Antarctica. In these cases, the mass loss amounts to an ensemble average of ~ 3.5 m sea-level equivalent by the year 3000 and ~ 5.3 m for the most sensitive experiment. Four phases of mass loss occur during the collapse of the West Antarctic Ice Sheet. For the reduced emissions pathway, the mean mass loss is ~ 0.24 m sea-level equivalent. By demonstrating that the consequences of the 21st century unabated warming path forcing are large and long-term, the results present a different perspective to ISMIP6 (Ice Sheet Model Intercomparison Project for CMIP6). Extended ABUMIP (Antarctic BUttrressing Model Intercomparison Project) simulations, assuming sudden and sustained ice-shelf collapse, with and without bedrock rebound corroborate a negative feedback for ice loss found in previous studies, where bedrock

*Present address: Institute of Low Temperature Science, Hokkaido University, Sapporo, Japan.

27 **rebound acts to slow the rate of ice loss.**

28 **1 INTRODUCTION**

29 The Antarctic ice sheet (AIS) contains more than half of the Earth's freshwater, enough to raise sea levels
30 by 58 metres (Fretwell and others, 2013). An ice mass of 7.4 mm sea-level equivalent (SLE) was lost from
31 the AIS between 1992 and 2017 (The IMBIE team, 2018), and there is evidence to suggest that parts of
32 the West Antarctic Ice Sheet (WAIS) may already have begun an irreversible retreat (Joughin and others,
33 2014; Rignot and others, 2014).

34 The possibility of WAIS retreat and collapse was first presented by Mercer (1968) and there is paleocli-
35 matic evidence that it collapsed during past warm periods (Pollard and DeConto, 2009; Alley and others,
36 2015; Dutton and others, 2015; Gasson and others, 2016; Turney and others, 2020). In contrast to the East
37 Antarctic Ice Sheet (EAIS), the WAIS is grounded on a bed that is mostly well below sea level (Fig. 1)
38 making it primarily a marine ice sheet. The WAIS bedrock bathymetry also deepens inward in many areas,
39 making it susceptible to marine-ice-sheet instability (e.g. Schoof, 2007). The WAIS is bounded by the two
40 largest ice shelf systems in the world, the Ross and the Ronne-Filchner, which currently act to buttress the
41 grounded ice sheet (e.g. Joughin and Alley, 2011) and reduce ice flow across long, below-sea-level grounding
42 lines.

43 To estimate the future sea-level-rise contribution from the Antarctic and Greenland ice sheets through
44 the end of the 21st century, the Coupled Model Intercomparison Project Phase 6 (CMIP6) (Eyring and
45 others, 2016) includes the Ice Sheet Model Intercomparison Project for CMIP6 (ISMIP6; Nowicki and
46 others, 2016, 2020). ISMIP6 uses output from Earth system models run under future emissions scenarios,
47 as atmospheric and oceanic forcing for ice-sheet models including the SIMulation CODE for POLythermal
48 Ice Sheets (SICOPOLIS; Greve and SICOPOLIS Developer Team, 2021) used here. The set-up and results
49 of the Antarctica ISMIP6 projections are described in Seroussi and others (2020), and the results specifically
50 obtained with SICOPOLIS are discussed in detail in Greve and others (2020). Using simulations from 13
51 international groups, ISMIP6 found an Antarctic mass loss that varied between -7.8 and 30.0 cm SLE from
52 2015 to 2100 under the "unabated warming path" of Representative Concentration Pathway (RCP) 8.5
53 (Seroussi and others, 2020). The WAIS mass loss varied greatly among the simulations with the greatest loss
54 simulated being 18.0 cm SLE, while the EAIS mass change varied between -6.1 and 8.3 cm. The results for

55 the RCP2.6 pathway (that represents substantial emissions reductions) lie within the uncertainty interval
56 of the results for RCP8.5. Payne and others (2021) compared the impact of CMIP5 and CMIP6 forcings
57 and found that the projected sea-level contribution at 2100 under the CMIP6 scenarios falls within the
58 CMIP5 range for the AIS. Edwards and others (2021) explored the uncertainty of the projections in greater
59 detail by using statistical emulation of the ice-sheet models, which allowed the consideration of a much
60 larger range of climate scenarios and forcings. This study essentially confirmed the ISMIP6 findings: By
61 2100, the AIS showed a response encompassing the range from a significant mass loss to a slight mass
62 gain due to the competing processes of increasing ice loss at and near the margins, and increased snowfall
63 accumulation.

64 While the ISMIP6 projections extend to the year 2100, other studies have investigated longer term AIS
65 change. To do this some have used statistical relationships between past temperatures and global sea levels
66 (Levermann and others, 2013; Schaeffer and others, 2012). Alternatively Golledge and others (2015) used
67 ice sheet models to demonstrate that atmospheric warming in excess of 1.5 to 2 °C above present, triggers
68 ice-shelf collapse and a centennial to millennial-scale response by the AIS. They simulated a contribution to
69 sea-level-rise from Antarctica under higher emission scenarios of 0.6 to 3 metres by the year 2300. Similarly
70 Garbe and others (2020) found that at greater than 2 °C of global average warming, the WAIS is committed
71 to long-term partial collapse. They also found distinct regimes in the rates of sea-level rise per degree, with
72 a doubling in the rate if warming becomes greater than 2 °C. Lipscomb and others (2021) used ISMIP6
73 forced sensitivity simulations extended to year 2500 under a constant climate to evaluate the Antarctic
74 response to ocean forcing. They found long-term retreat of the WAIS and showed that the Amundsen sector
75 exhibits threshold behaviour with modest retreat or complete collapse depending on parameter settings
76 in the melt scheme, ocean forcing, and basal friction law. Complete collapse of the WAIS occurred under
77 some combinations of low basal friction and high thermal forcing anomalies. The Antarctic BUttressing
78 Model Intercomparison Project (ABUMIP; Sun and others, 2020) compared ice-sheet model responses to
79 a removal of ice-shelf buttressing by investigating the response to sudden and sustained loss of ice shelves
80 and found that the WAIS contributed 1.91 to 5.08 m sea-level rise due to marine ice-sheet instability over
81 the 500 year long simulations. These studies point to threshold behaviour in the WAIS in response to
82 atmosphere and ocean warming.

83 The goal of our study is to investigate the extended effects of the climate projections used in ISMIP6.
84 To do this we simulate the evolution of the AIS until the year 3000. Until 2100, we follow the ISMIP6

85 protocol, whereas afterwards we assume a steady, late-21st-century climate without any further trend.
86 In this longer-term perspective, a very different picture emerges compared to the 21st century ISMIP6
87 findings. The remainder of this paper is divided into four sections. Firstly the methods are outlined in
88 Section 2, followed by an analysis of the simulations in Section 3. Thirdly, the results are evaluated in
89 Section 4, and finally a summary is provided in Section 5.

90 2 METHODS

91 SICOPOLIS, a polythermal ice-sheet model originally created by Greve (1995, 1997), is used to extend the
92 ISMIP6 experiments to the year 3000. Here, we use version 5-dev, revision develop_63_rv5.1-62-g3c25a05
93 (Greve and SICOPOLIS Developer Team, 2021). The simulation set-up for ISMIP6 is described in Greve
94 and others (2020) and only summarized here. The model domain covers the entirety of Antarctica on
95 an 8 km horizontal resolution regular (structured) grid based on a polar stereographic projection, with 81
96 terrain-following ice layers and 41 lithosphere layers. Hybrid shallow-ice-shelfy-stream dynamics, in the
97 modified form of Bernales and others (2017), is used for grounded ice, and the shallow-shelf approximation
98 (SSA) is used for floating ice. We employ a Weertman-Budd-type sliding law that accounts for sub-
99 melt sliding and the subglacial water-layer thickness (Greve and others, 2020, their Eqs. (7), (8), and
100 accompanying text). This sliding law includes the effective (ice minus water) basal pressure, assumed to
101 be equal to the weight of the ice column above buoyancy. Therefore, the basal drag is continuous across
102 the grounding line (approaches zero from the grounded side, equal to zero everywhere under floating ice).
103 Gladstone and others (2017) performed numerical experiments with the Elmer/Ice model in full-Stokes
104 mode for a simplified rectangular domain of a marine ice sheet, testing horizontal resolutions of 1.8, 3.6
105 and 7.2 km. They demonstrated that, with a Weertman-Budd-type sliding law similar to ours, 7.2 km
106 resolution (similar to our 8 km) is sufficient to produced good results for the grounding line migration in
107 both advance and retreat scenarios. By contrast, for a Weertman-type law that disregards the effective
108 pressure and features a discontinuity of the basal drag across the grounding line, even 1.8 km does not lead
109 to an acceptable convergence of the grounding line migration. We therefore consider our 8 km resolution,
110 in combination with the Weertman-Budd-type sliding law, as sufficient for modelling marine ice sheet
111 dynamics, including grounding line migration, with reasonable accuracy.

112 The main physical parameters are listed in Table 1. A paleoclimatic spin-up simulation is run over a
113 full glacial cycle (140 ka) to the year 1990 as described in Greve and others (2020, Sect. 3.2). The basal

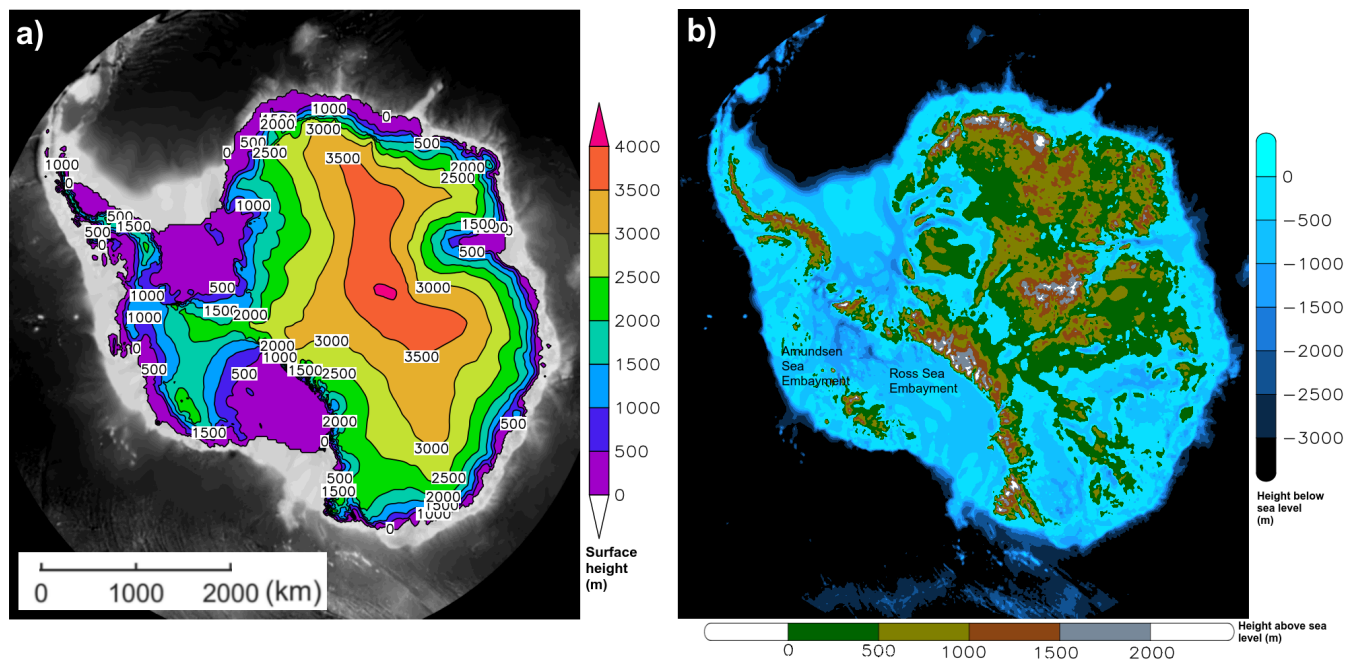


Fig. 1. SICOPOLIS year 2015 a) simulated surface topography and b) bedrock elevation above and below sea level. The bedrock elevation is from Bedmap2 (Fretwell and others, 2013) mapped onto the 8 km grid.

114 sliding coefficient is chosen differently for the 18 IMBIE (Ice sheet Mass Balance Inter-comparison Exercise)
 115 2016 basins (Rignot and Mouginot, 2016) to optimize the agreement between simulated and observed 1990
 116 surface velocities (Greve and others, 2020, Sect. 3.2.3). Simulated vs. observed ice thicknesses and surface
 117 velocities are shown in their Figures 5 and 6.

118 To obtain the initial state of the ice sheet shown in Figure 1a, there are then 25 years remaining to get
 119 to the year 2015, which marks the start date of the ISMIP6 projections. Therefore, an additional simulation
 120 referred to as “Historical” in Figure 2 is run that applies NorESM1-M RCP8.5 surface mass balance, surface
 121 temperature anomalies, and oceanic forcing (discussed in more detail below), to the 1960–1989 climatology
 122 (Greve and others, 2020, Sect. 4.1).

123 The ISMIP6 projections run from 2015 to 2100 with annually-averaged atmospheric forcing consisting of
 124 anomalies of surface mass balance and temperature from a 1995 to 2014 climatology (Barthel and others,
 125 2020; Nowicki and others, 2020; Seroussi and others, 2020; Payne and others, 2021). After 2100, the
 126 annual atmospheric forcing for the 10-year interval 2091–2100 is randomly sampled such that no further
 127 warming trend is applied (similar to Calov and others, 2018) but some year to year variability remains.
 128 With the surface mass balance and temperature fixed on this 10-year period, they remain unchanged even
 129 if the topography of ice changes over the remaining 900 years. Ice-shelf basal melt rates are calculated

Table 1. Physical parameters used for the simulations of this study.

Quantity	Value
Density of ice, ρ	910 kg m ⁻³
Density of sea water, ρ_{sw}	1028 kg m ⁻³
Gravitational acceleration, g	9.81 m s ⁻²
Length of year, 1 a	31 556 926 s
Power-law exponent, n	3
Residual stress, σ_0	10 kPa
Flow enhancement factor, E	grounded ice: 5, floating ice: 1
Melting temperature at low pressure, T_0	273.16 K
Clausius-Clapeyron gradient, β	8.7×10^{-4} K m ⁻¹
Universal gas constant, R	8.314 J mol ⁻¹ K ⁻¹
Heat conductivity of ice, κ	$9.828 e^{-0.0057 T[\text{K}]} \text{ W m}^{-1}\text{K}^{-1}$
Specific heat of ice, c	$(146.3 + 7.253 T[\text{K}]) \text{ J kg}^{-1}\text{K}^{-1}$
Latent heat of ice, L	$3.35 \times 10^5 \text{ J kg}^{-1}$
Sliding coefficient, C_b^0 *	Range from 0.1 to $2.7621 \text{ m a}^{-1} \text{ Pa}^{-1}$
Sliding exponents, (p, q) *	(3, 2)
Sub-melt-sliding parameter, γ *	1°C
Coefficient for water-layer-enhanced basal sliding, c^*	9
Threshold water-layer thickness, H_w^0 *	5 mm
Density \times specific heat of the lithosphere, $\rho_l c_l$	$2000 \text{ kJ m}^{-3}\text{K}^{-1}$
Heat conductivity of the lithosphere, κ_l	$3 \text{ W m}^{-1}\text{K}^{-1}$
Thickness of the thermal upper boundary layer of the lithosphere, H_{lt}	2 km
Flexural stiffness of the lithosphere, K_l	10^{25} N m
Asthenosphere density, ρ_a	3300 kg m^{-3}
Time lag for the relaxing asthenosphere, τ_a	3000 a

*: For details of the Weertman-Budd-type sliding law with sub-melt sliding and hydrology, see Greve and others (2020, their Eqs. (7), (8), and accompanying text).

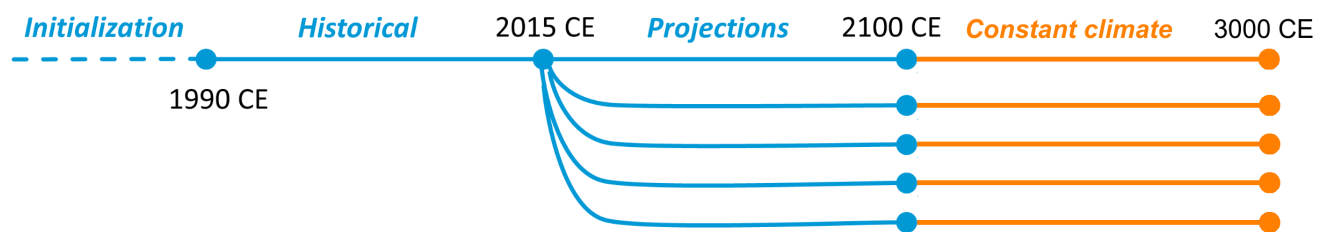


Fig. 2. Experimental design. Initialization is followed by a historical simulation from 1990 until 2015. ISMIP6 projections run from 2015 until the end of 2100. From 2100 to 3000 no additional forcing is applied. (Credit: edit of Figure 1 in Greve and others (2020), originally by Martin Rückamp, AWI Bremerhaven, Germany.)

130 using the non-local quadratic melt-rate parameterization of the “ISMIP6 standard approach”, driven by
 131 extrapolating the oceanic thermal forcing into the ice-shelf cavities (Jourdain and others, 2020). Beyond
 132 2100, it is kept fixed at 2100 values.

133 All simulations are listed in Table 2. Fourteen experiments are for the 21st century “unabated warming
 134 path” RCP8.5 (CMIP5) / SSP5-8.5 (Shared Socioeconomic Pathways, CMIP6), and three are for the
 135 RCP2.6/SSP1-2.6 pathway that represents substantial emissions reductions and a maintenance of the
 136 global mean temperature below a 2 °C increase. In addition a control simulation (‘ctrl_proj’) uses constant
 137 climate conditions based on a 1995–2014 climatology and the present day oceanic forcing.

138 Using the NorESM1-M RCP8.5 forcing, “High” and “Low” sub-ice-shelf melt-rate calibrations are
 139 tested, as well as a calibration (“PIGL-medium”) that applies observed basal-melt rates near the ground-
 140 ing line of the Pine Island ice shelf under all ice shelves (Jourdain and others, 2020). One experiment,
 141 “CCSM4/RCP8.5 ice-shelf collapse”, attempts to parameterize the complex processes of surface melting
 142 and hydrofracture by implementing a time-dependent ice-shelf-collapse mask. It assumes that collapse
 143 occurs following a 10-year period with annual surface melt above 725 mm (Trusel and others, 2015).

144 In addition to the extended ISMIP6 simulations, the Antarctic BUttrressing Model Intercomparison
 145 Project (ABUMIP; Sun and others, 2020) simulations are also extended to the year 3000. ABUMIP
 146 compares ice-sheet model responses to a removal of ice-shelf buttressing by investigating the scenario of
 147 sudden and sustained loss of all ice shelves. This experiment was designed to show the full (if unrealistic)
 148 potential of marine-ice-sheet instability. The experiments are initialized from the same simulated 1990
 149 state of Antarctica discussed above. The original ABUMIP simulations were run for 500 years and here we
 150 extend them an additional 500 years. The simulations are run with and without bedrock rebound (glacial
 151 isostatic adjustment). For ABUMIP there are five experimental set-ups as summarized below (for further

Table 2. ISMIP6 future climate experiments discussed in this study. See Nowicki and others (2020) for references for the GCMs and Greve and others (2020) for further detail on the SICOPOLIS application of the experiments.

CMIP5 simulations		
Scenario	GCM	Ocean forcing
RCP8.5	NorESM1-M	Medium
RCP8.5	MIROC-ESM-CHEM	Medium
RCP2.6	NorESM1-M	Medium
RCP8.5	CCSM4	Medium
RCP8.5	NorESM1-M	High
RCP8.5	NorESM1-M	Low
RCP8.5	CCSM4 (ice-shelf collapse)	Medium
RCP8.5	NorESM1-M	PIGL-Medium
RCP8.5	HadGEM2-ES	Medium
RCP8.5	CSIRO-Mk3.6.0	Medium
RCP8.5	IPSL-CM5A-MR	Medium
RCP2.6	IPSL-CM5A-MR	Medium
CMIP6 simulations		
SSP5-8.5	CNRM-CM6-1	Medium
SSP1-2.6	CNRM-CM6-1	Medium
SSP5-8.5	UKESM1-0-LL	Medium
SSP5-8.5	CESM2	Medium
SSP5-8.5	CNRM-ESM2-1	Medium
Control simulation		
None (ctrl_proj)	1960-1989 climatology	Medium

152 detail see Sun and others, 2020):

153 (1) Control run (abuc): 1990 (initial) forcing is applied for the duration of the simulation.

154 (2) Ice-shelf removal or ‘float-kill’ (abuk) with no bedrock rebound: All floating ice is removed at the
155 simulation start and then continuously throughout the simulation. The bed topography remains fixed
156 at 1990 levels.

157 (3) Ice-shelf removal or ‘float-kill’ with bedrock rebound (abukiso): The same experiment as in (2) but
158 including glacial isostatic adjustment (GIA) using an elastic-lithosphere-relaxing-asthenosphere (ELRA)
159 model (parameters by Sato and Greve, 2012).

160 (4) Extreme sub-shelf melt and no bedrock rebound (abum): Applies an extremely high melt rate of
161 400 m a^{-1} underneath floating ice for a period of 500 years. This experiment acts as an alternative
162 to the more extreme abuk and also inevitably leads to a rapid loss of all ice shelves.

163 (5) Extreme sub-shelf melt with bedrock rebound (abumiso): As experiment (4) but including GIA as in
164 (3).

165 **3 RESULTS**

166 **3.1 Extended ISMIP6 experiments**

167 For the ISMIP6 extended experiments, the SLE contribution due to ice-mass melt is shown in Figure 3.
168 The graph is divided into 4 phases to roughly designate periods where the rates of SLE change tend to be
169 relatively constant. Over the ISMIP6 original experiment range, which ends at 2100 (within phase 1), there
170 is a small, and uncertain, contribution to SLE. Throughout the 21st century, the experiments are identical
171 to those for ISMIP6; see Greve and others (2020, Sect. 4.2) for a detailed discussion. Beyond 2100, under
172 a no-longer warming climate, the high-emission scenarios transition to a period of relatively constant SLE
173 change (phase 2). The onset of phase 2 varies between the cases from the latter half of the 21st century to
174 the early 22nd century. A third phase then begins as the rate of SLE contribution increases. This phase is
175 the period of most rapid ice-sheet mass-loss and there is a fair degree of variability between the simulations
176 in both the timing of the transition from phase 2 to 3 (between years 2340 and 2560), and in the level of
177 SLE contribution at which this phase begins. A fourth and final phase then begins as the SLE contribution
178 levels out, which on average produces an end SLE contribution for the high-emissions cases of $\sim 3.5 \text{ m}$ by

179 the year 3000. Most of the cases are clustered close to this value with all but two within ± 0.4 m of the
180 final average SLE. This is similar to a ~ 3.3 m value found in Bamber and others (2009) who calculated
181 the potential SLE contribution due to WAIS collapse by identifying grid cells below sea level on retrograde
182 bed slopes to infer the limit of grounding line retreat.

183 To investigate the causes of these apparent ice-sheet mass-loss regime shifts between the four phases,
184 here we analyse a representative case in more detail. The MIROC-ESM-CHEM RCP8.5 case lies within the
185 cluster of cases close to the mean of the unabated 21st century warming (RCP8.5/SSP5-8.5) runs (Fig. 3).
186 For this case the phase onsets occur for phase 2 around ~ 2100 , phase 3 around ~ 2350 and phase 4 at
187 ~ 2500 . The physical controls on the similar phases in other experiments are the same.

188 Figure 4 shows that simulated ice-mass loss is dominated by WAIS change and it is here where the
189 causes of the phase changes can be found. The transition from phase 1 to phase 2 is associated with the
190 period when the Ross Ice Shelf has retreated to such a point that the Ross Sea Embayment begins a more
191 rapid ice loss due to a reduction in the buttressing from the ice shelf (Fig. 4b). The transition to phase
192 3 occurs as, in addition to continued Ross Sea Embayment mass loss, the Amundsen Sea Embayment
193 begins a rapid retreat along its inward sloping grounding lines (Fig. 4c). Phase 4 is then associated with a
194 levelling-off in the SLE contribution as the WAIS is reduced to such an extent that the loss of the remaining
195 ice grounded below sea level begins to contribute less and less to the SLE contribution (Fig. 4d-f).

196 In Figure 4 cross-sections through the ice along two connected diagonals through the WAIS are shown
197 for the 6 times in the side panels a-f. This cross-section presents a roughly flow-line oriented view from the
198 Ronne-Filchner Ice Shelf on the left, where minimal melt occurs, to the Ross Ice Shelf on the right where
199 collapse occurs.

200 The greatest change to the topography in the cross-section occurs between the year 2395 and 2595
201 cross-sections during which time a large ice shelf develops above a retrograde slope in the bed topography.
202 The outer edge of this ice shelf lies inward of the original Ross Ice Shelf area which is now devoid of ice.
203 It is also during this period when the peak elevation of the cross-section drops by about 400 m with very
204 little change either before or after. This time period coincides with when the retreat from the Amundsen
205 Embayment and the Ross Sea Embayment meet over the Bentley subglacial trench.

206 An alternative cross-section across the WAIS that includes part of the EAIS is shown in Figure 5 (cross-
207 section location on inset in panel b) for four years that are chosen to highlight the key phases of retreat. At
208 the initialization time (2015, Fig. 5a) the WAIS is grounded on bedrock with just a sliver of ocean in the

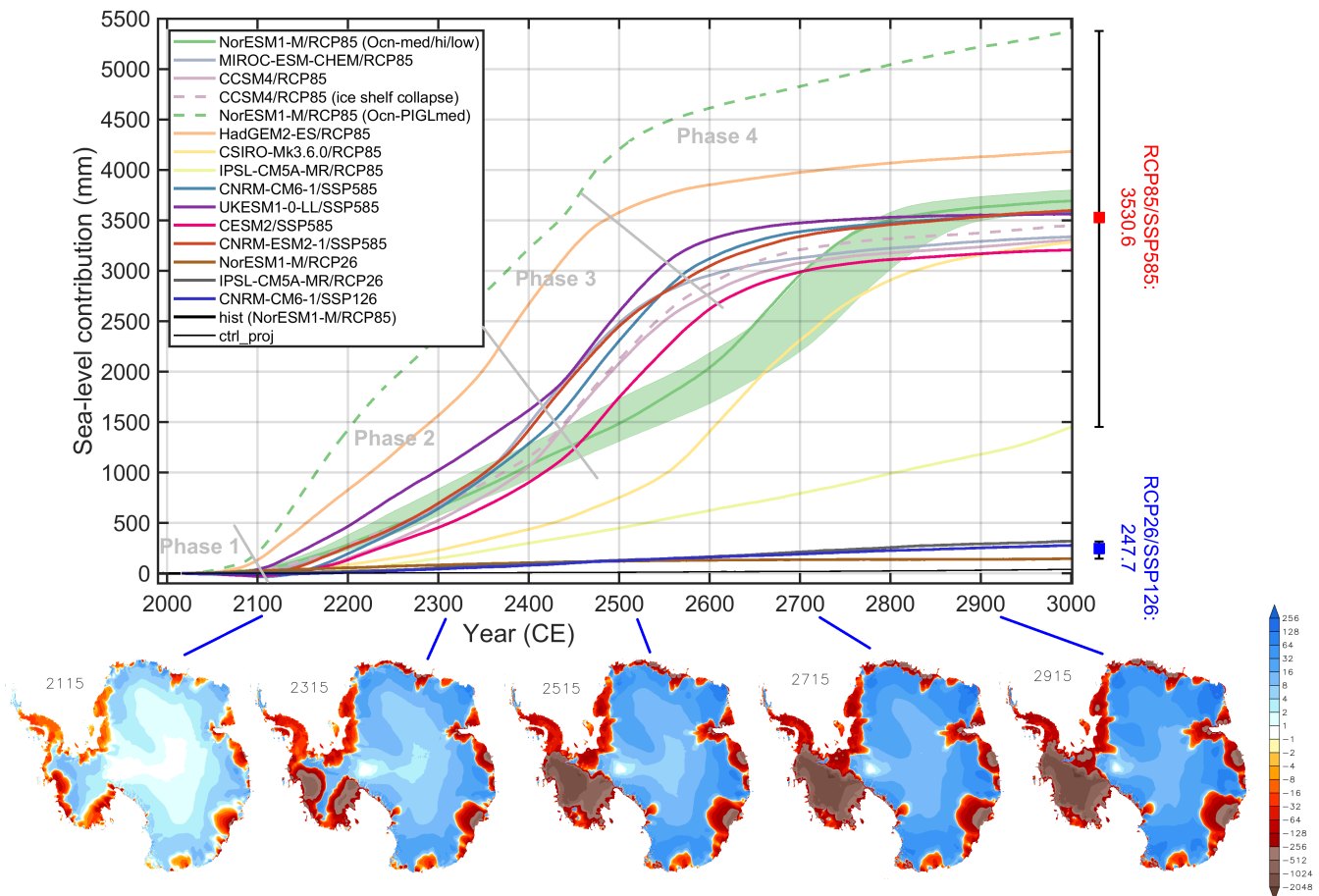


Fig. 3. Simulated ice mass change, counted positively for loss and expressed as sea-level equivalent (SLE) contribution. Phases mentioned in the text are labeled and diagonal grey lines are rough guides to denote the phase transitions. The red and blue boxes to the right show the means for RCP8.5/SSP5-8.5 and RCP2.6/SSP1-2.6, respectively; the whiskers show the full ranges. Map-view plots below are ice surface elevation differences from 2015 (m) for the year indicated for case MIROC-ESM-CHEM RCP8.5.

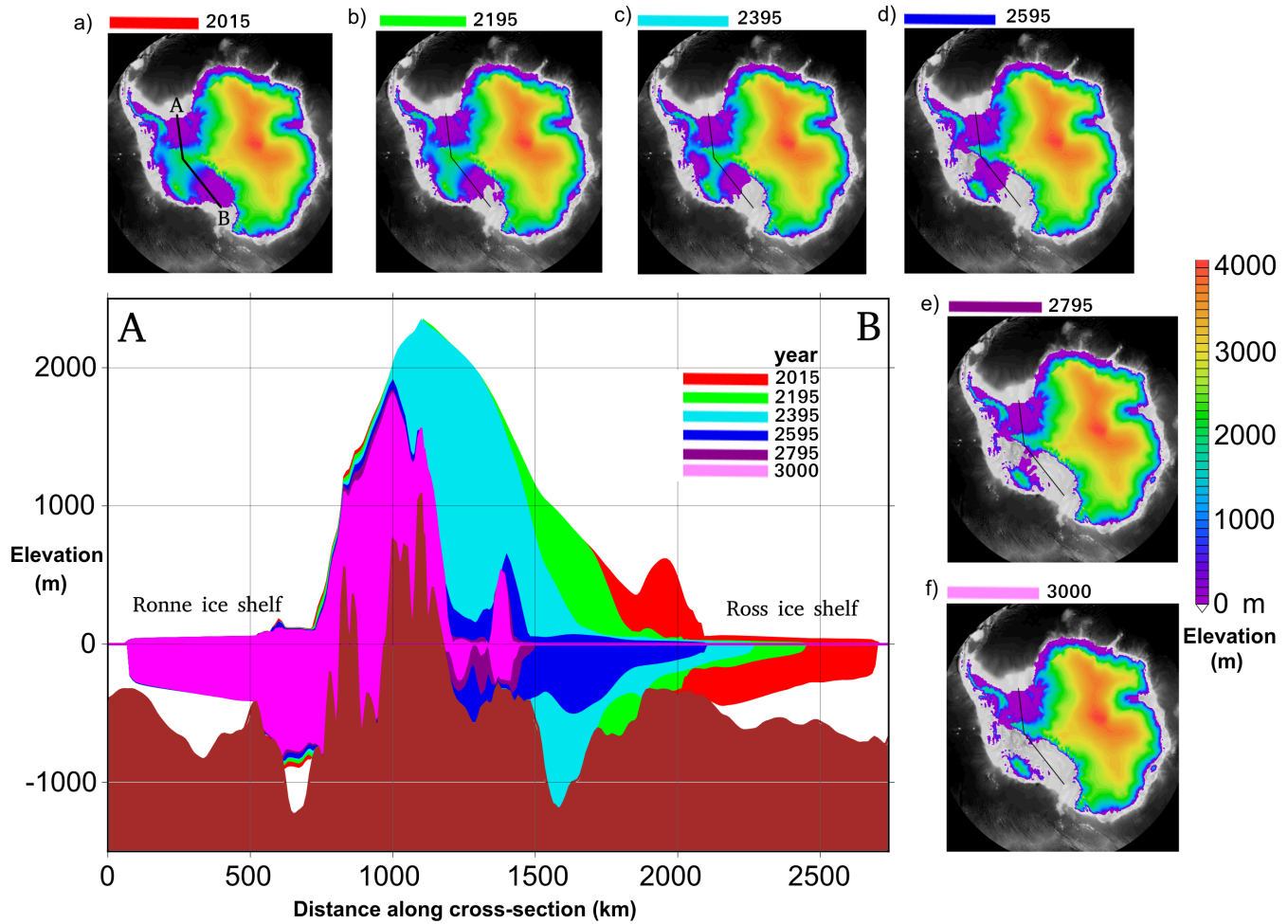


Fig. 4. West Antarctica vertical cross-section for simulation MIROC-ESM-CHEM RCP8.5 showing the colour-coded ice extent for the years labeled in the side plots (a to f) that show the ice surface elevation for the year indicated.

209 middle where the cross-section crosses the deep interior of the Ross Ice Shelf. During phase 1 the ice-sheet
210 profile changes little, then during phase 2, ocean melting undercuts the WAIS from the Ross Ice Shelf into
211 the Ross Sea Embayment. The surface elevation drops rapidly where this undercutting occurs, as shown
212 for 2395 in Figure 5b. As the Amundsen Sea Embayment also loses ice, the central WAIS ridge becomes
213 narrower.

214 During phase 3 the central ridge then collapses as ice mass is evacuated due to the compounding losses
215 from the Amundsen and Ross Sea Embayments. Phase 3 transitions to phase 4 not when all the WAIS ice
216 has melted but rather when the ice mass has been reduced to such an amount that further melt contributes
217 little to sea level as indicated in Figure 5c. Beyond that the remainder of WAIS ice, now mostly detached
218 from the bedrock can melt while contributing little to sea level in phase 4. Therefore the rate of mass loss
219 levels off quickly after most of the remaining ice in the WAIS is at or very nearly at flotation. The EAIS
220 exhibits very little change in the cross-section and the slight thickening is evident on very close inspection.

221 A cross-section through the Amundsen Embayment from the Pine Island Glacier and Thwaites Glacier
222 area up to the WAIS ridge is shown in Figure 6. The greatest loss of ice is seen between the year 2195 and
223 2595 sections however the greatest ice edge retreat is between year 2395 and 2795 because of the formation
224 of ice shelves, the most prominent of which is seen in the year 2395 cross-section. The initial ice shelf, the
225 year 2395 ice shelf, and another at year 2595 all appear to be related to shallow areas in the bedrock that
226 act to pin the shelf and restrain the ice behind. The precarious nature of the present day ice extent is
227 evident in the drop in bedrock from the ice edge to about 490 km along the section.

228 The bedrock in the cross-section is plotted for year 2015. By the latter stages in the simulation the
229 bedrock has lifted slightly, and the apparent narrow undercut in the ice seen in year 2795 and 3000 between
230 800 and 900 km along the cross-section, is a consequence of this uplift rather than representing sea water
231 undercutting the ice.

232 A comparison between the three low-emission simulations with their high-emission counterparts is made
233 in Figure 7. For all of the low-emission cases there is very little noticeable change in the topography of the
234 ice sheet as a whole, consistent with the only small contribution to sea-level from these cases (Fig. 3). For
235 the high-emission cases, all show large losses in the WAIS with the greatest losses seen in the only CMIP6
236 case of the three, the CNRM-CM6 SSP5-8.5, which is also the only case that loses the Ronne-Filchner Ice
237 Shelf. This is because the ocean in this sector is relatively warmer in the ISMIP6 forcing from the CMIP6
238 projections. The two CMIP5 RCP85 cases, the NORESM1-M and IPSL-CM5A-MR, are quite different

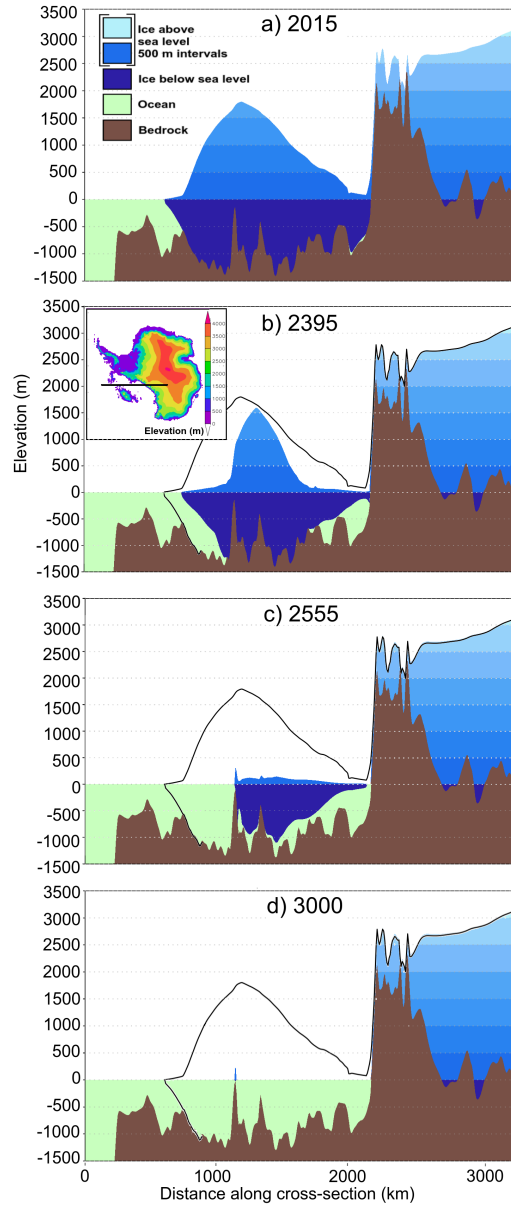


Fig. 5. Ice cross-sections for simulation MIROC-ESM-CHEM RCP8.5 for a) 2015, b) 2395, c) 2555, and d) 3000 across the black line shown on inset panel of b). In b), c), and d) the black line indicates the 2015 ice profile.

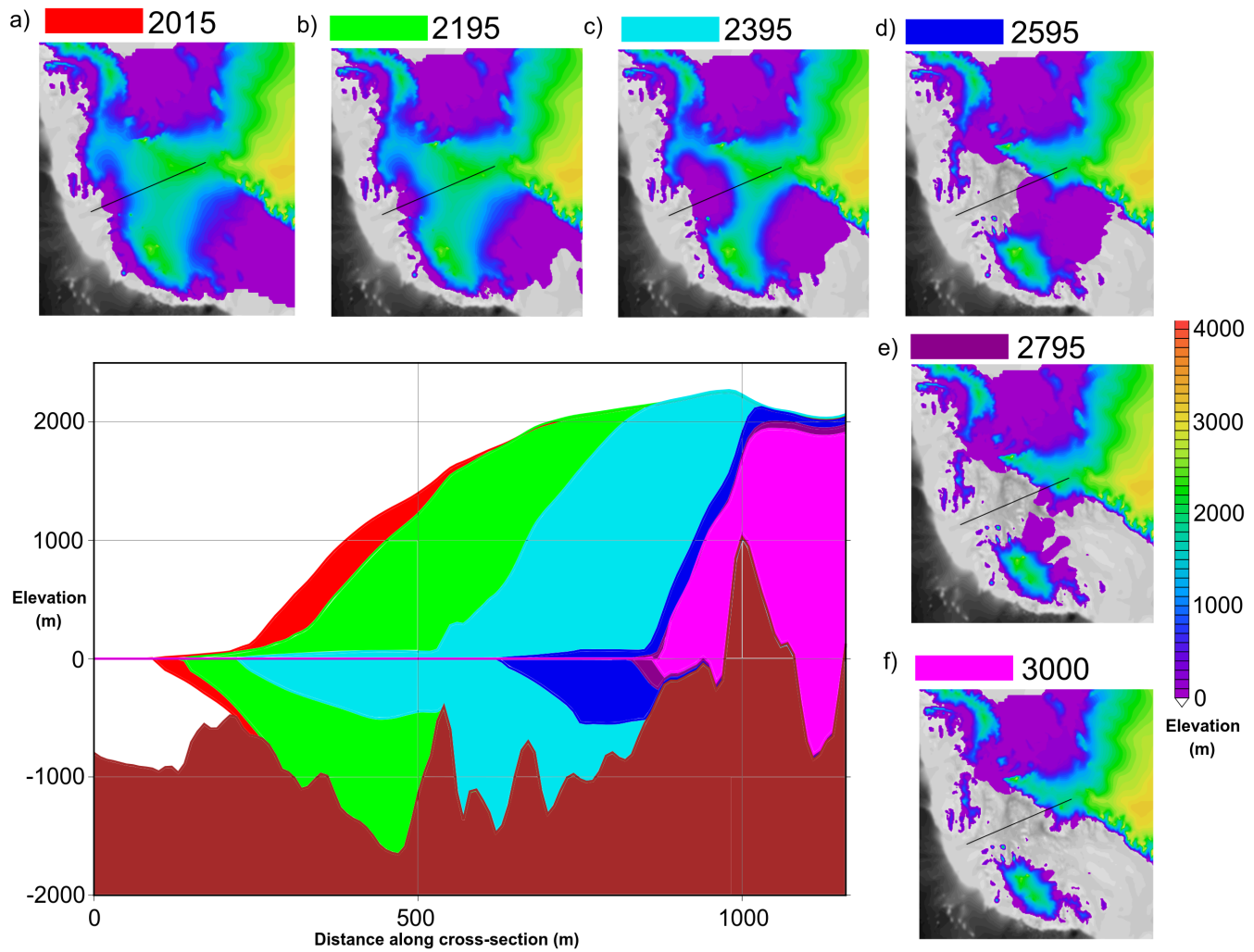


Fig. 6. Amundsen Embayment cross-section for simulation MIROC-ESM-CHEM RCP8.5 showing the ice extent for the years labeled in the side plots (a-f) which show the ice surface elevation for the year indicated.

239 from each other with the NORESM1-M suffering much greater WAIS loss.

240 In Figure 8 the sea-level contributions by year 3000 are shown for each of 3 regions. Averaged across
241 all the high-emission cases, the WAIS contributes 3.2 m SLE compared with just 0.26 m from the EAIS
242 and 0.0044 m from the Antarctic Peninsula. This contrasts with the low-emission cases which have average
243 SLE contributions from the WAIS and EAIS of 0.086 and 0.12 m respectively, with the Antarctic Peninsula
244 contribution being very slightly negative at -0.0020 m SLE.

245 In addition to the standard ISMIP6 simulation set up, which includes a “medium” ice-shelf basal melt
246 calibration, two additional simulations under the NorESM1-M/RCP8.5 atmospheric forcing are run with
247 “high” and “low” ice-shelf basal melt calibrations. The results are shown by the green line (“medium”) and
248 green-shaded region (“high” is the top edge of the shading and “low” the bottom) in Figure 3. Decreasing
249 the ice-shelf basal melt causes a delay in the onset of the phase transitions when comparing “high” and
250 “low”, which produces a maximum sea-level contribution difference between “high” and “low”, during early
251 phase 4, of ~ 70 cm. The “medium” (standard) case behaves slightly differently, lining up closely with the
252 “high” case during early phase 4. Despite these differences all calibrations gradually converge during phase
253 4 such that the sea-level contributions end up only ~ 20 cm different by year 3000.

254 A more extreme test is NorESM1-M RCP8.5 with the “PIGL-medium” calibration. In this case phase
255 2 onset begins earlier than the other cases and lies well within the 21st century during the original ISMIP6
256 simulation period. As noted in Greve and others (2020), “It has a pronounced effect on the mass loss of
257 the ice sheet: By 2100, it is 216.7 mm SLE compared to the initial 1990 state”. In this case the transition
258 between phase 2 and 3 is unclear or absent and, while there is some slowing to the increase in sea-level
259 contribution marking phase 4, sea-level contribution continues to increase at a relatively constant rate such
260 that by the year 3000 its total contribution is 5.4 m, the greatest of any of the cases. The reason for this
261 greater and continuing loss is in part because this case produces EAIS losses in the Amery and Wilkes
262 basins that are ongoing by the simulation end.

263 **3.2 Extended ABUMIP experiments**

264 For the extended ABUMIP simulations, ice thicknesses at the end of the simulations are shown in Figure 9.
265 The ice-shelf removal (abuk, abukiso) and extremely high ice-shelf melt (abum, abumiso) both result in
266 great changes to the ice sheet. In contrast to the extended ISMIP6 simulations, there are considerable
267 losses in the EAIS in some of the regions where the ice is grounded below sea level. All extended ABUMIP

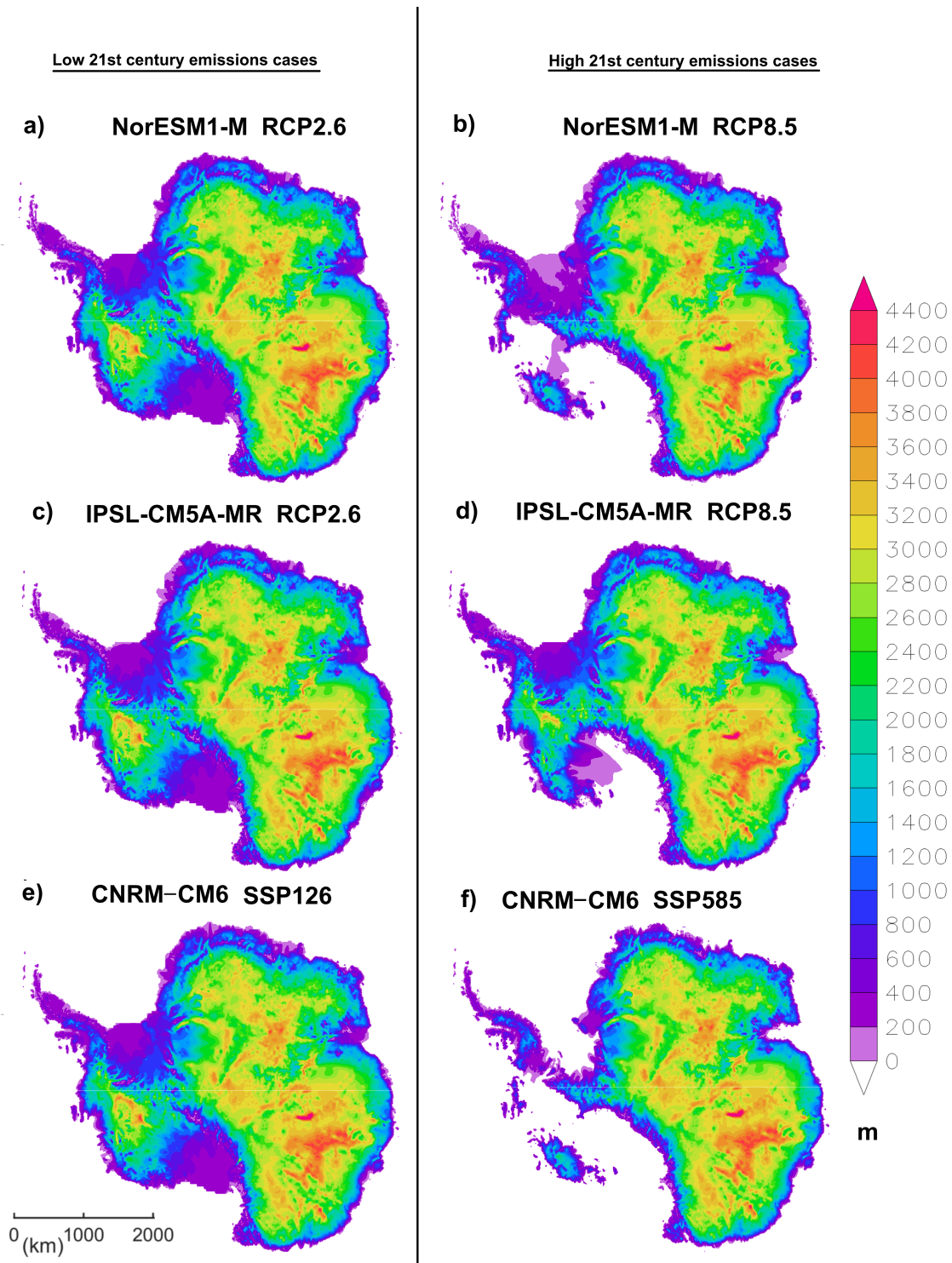


Fig. 7. Ice thickness at year 3000 for emissions reduction cases (left) and their counterpart high-emission cases (right).

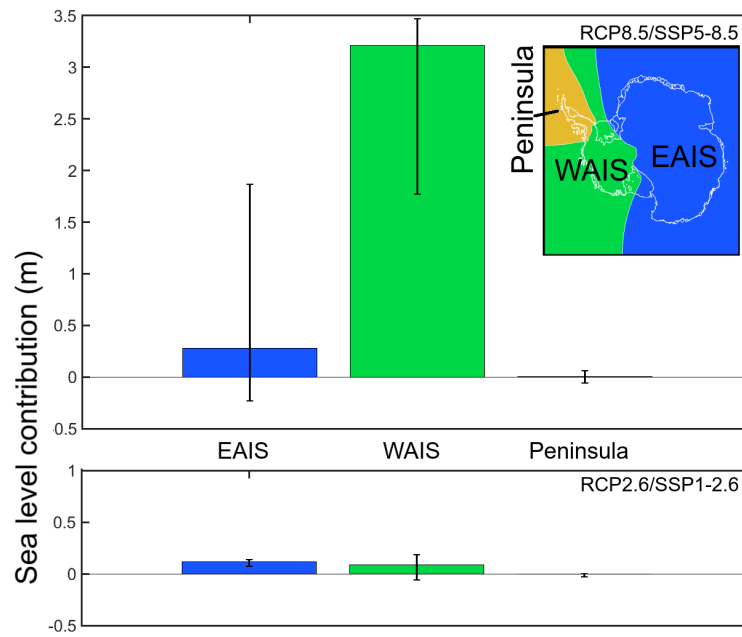


Fig. 8. Sea-level equivalent contribution from 3 regions (shown in top right) by year 3000 relative to ctrl_proj averaged across all the high (RCP8.5/SSP5-8.5, top) and low (RCP2.6/SSP1-2.6, bottom) emission cases. The whiskers show the full range of sea-level contributions across the simulations that make up the average.

268 simulations produce retreat inwards from the Amery Ice Shelf, however only in abum and abumiso is there
 269 a substantial retreat in the Wilkes Basin. These regions of greatest retreat are consistent with the original
 270 ABUMIP experiments in Sun and others (2020, Figs. 2 and 3) while being somewhat expanded given the
 271 longer simulation period.

272 Both the float kill, and extreme ice shelf melt cases were run with (abumiso, abukiso), and without,
 273 bedrock rebound (abum, abuk). Bedrock rebound occurs during, and after, ice-sheet mass loss, with the
 274 greatest amount reaching ~ 200 m of lift in central West Antarctica shown in Figure 10. The Aurora
 275 Basin, in particular, shows a large difference in ice-sheet loss with and without rebound (Fig. 9a,b), yet it
 276 experiences less rebound than other areas of major ice loss.

277 In fact the greatest differences in ice-sheet geometry develop over the EAIS, and this seems to be due
 278 to the slower response of the ice sheet compared to the WAIS allowing a greater cumulative impact from
 279 rebound to develop. In Figure 10 the velocity difference due to rebound indicates large regions where
 280 bedrock rebound has slowed surface velocities in the Aurora Basin and also the Amery, Slessor, Recovery,
 281 and Foundation basins. The potential mechanisms responsible for these differences are considered in the
 282 discussion below.

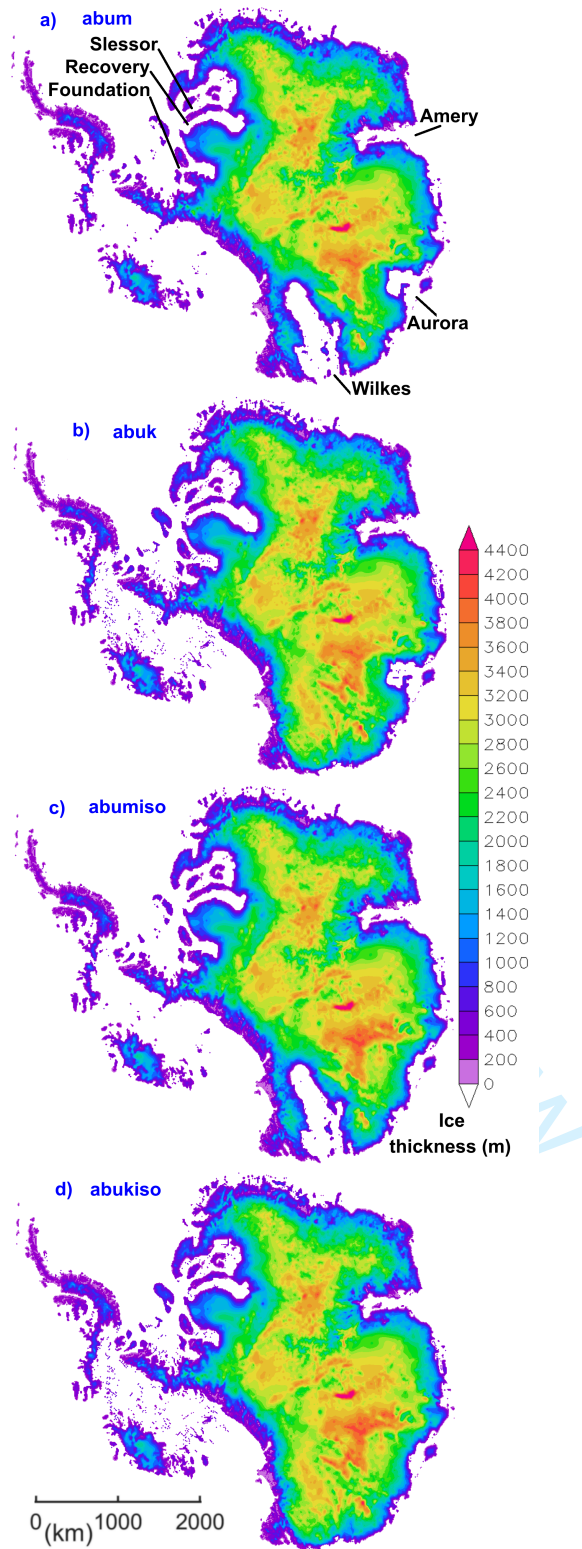


Fig. 9. ABUMIP ice thickness for year 3000 for a) abum, b) abuk, c) abumiso, and d) abukiso.

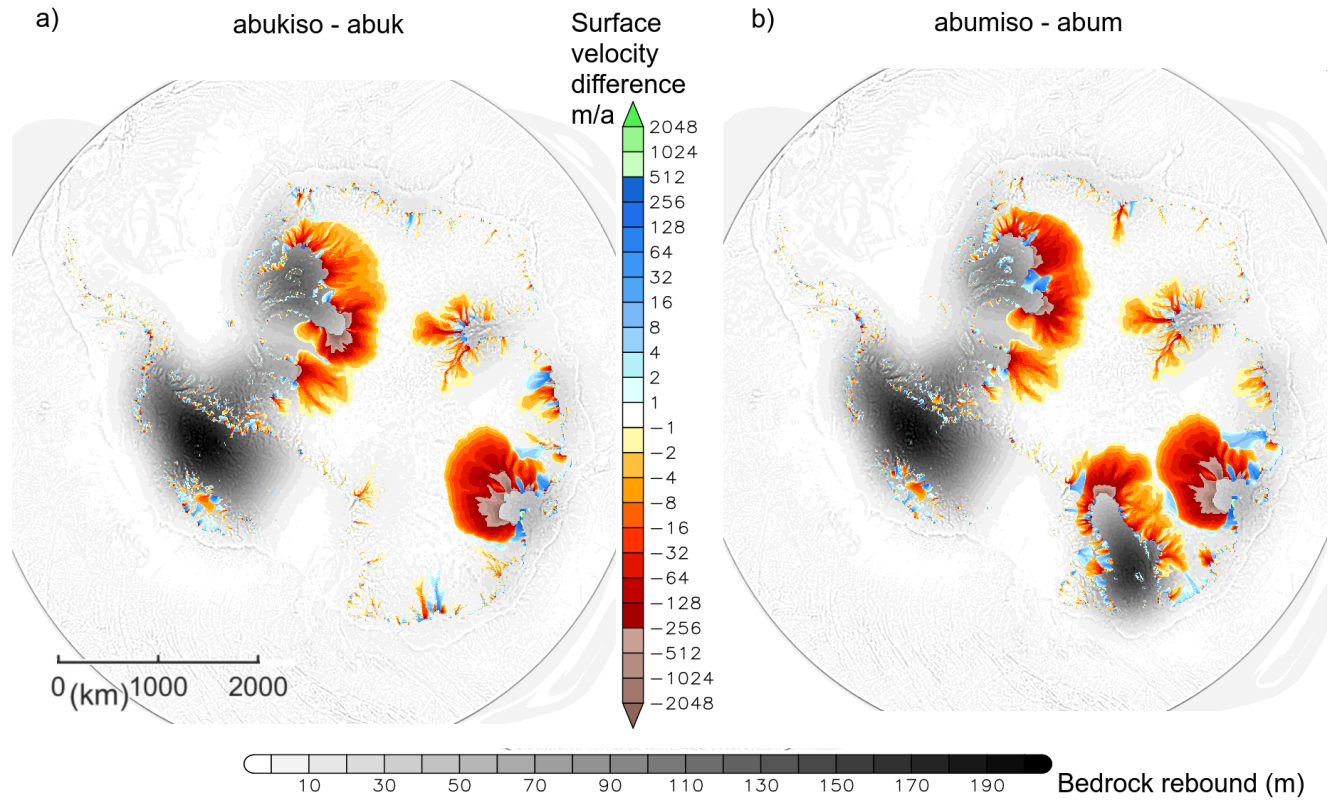


Fig. 10. Surface velocity differences between the ABUMIP bedrock rebound cases and the no rebound cases for the final simulation year (1000 years from 1990). Velocity differences are only plotted where ice exists in both the simulations. Underlain in gray shades is the bedrock rebound for a) abukiso and b) abumiso.

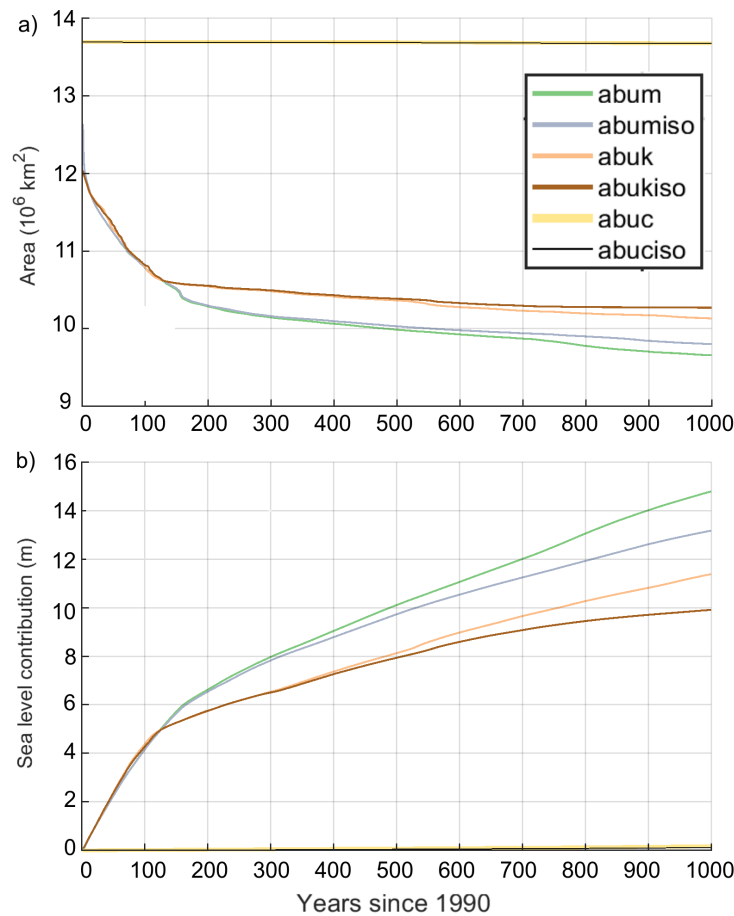


Fig. 11. ABUMIP a) total (grounded + floating) ice area and b) sea-level equivalent contribution.

283 The cases without rebound gradually lose a greater area of ice over the course of the simulations and
 284 end up with $\sim 1.5 \times 10^5 \text{ km}^2$ less ice sheet area (Fig. 11a). Overall the cases with rebound lose about 1.5
 285 metres less SLE (Fig. 11b).

286 4 DISCUSSION

287 The extended ISMIP6 experiments show the simulated long-term effect of applying a climate based on the
 288 last 10 years of the 21st century from the unabated warming and reduced emissions climate change scenarios.
 289 The simulations apply the assumption of no climate warming or cooling beyond year 2100. While using the
 290 same climate forcing data from ISMIP6, the long-term picture is different from the 21st century ISMIP6
 291 experiments showing that it is only in the long term that the consequence of different 21st century emission
 292 scenarios becomes strikingly apparent. Under the unabated warming scenario, the AIS undergoes ice mass
 293 loss primarily in the WAIS with the rate of loss divided into the 4 phases as detailed in the results above.

294 SICOPOLIS is rather insensitive to the applied climate forcing in the Amundsen Embayment due to the
295 applied surface mass balance correction which has additional accumulation to prevent the Thwaites/Pine
296 Island glaciers from becoming unstable before the end of the spin-up simulations. This issue is related to
297 the model SICOPOLIS and not a general deficiency in the ISMIP6 forcing. It is possible that this reduces
298 the rate of ice-sheet collapse in the Amundsen Embayment as compared to in the Ross Sea Embayment.
299 Regardless, SICOPOLIS appears to be simulating a marine-ice-sheet instability in these regions where the
300 bed has a reverse slope and an initial retreat increases discharge while reducing the balance flux, leading
301 to grounding line thinning and further retreat (e.g. Schoof, 2007). In the reduced emission scenarios the
302 WAIS collapse does not occur indicating that a climate threshold for large WAIS loss exists and that the
303 2091-2100 forcing in the reduced emission cases is below this threshold. To clarify, this result is specific
304 to the SICOPOLIS results presented here and could be substantially different with other setups that may
305 trigger marine-ice-sheet instability in the WAIS even under constant present day conditions. The most
306 important negative feedback opposing these positive feedbacks is due to increased precipitation in warming
307 temperatures which has been both observed (e.g. Frieler and others, 2015) and projected for the future,
308 over the Antarctic continent (Krinner and others, 2007; Uotila and others, 2007; Ligtenberg and others,
309 2013). Other negative feedbacks on ice loss include self gravitation and isostasy.

310 Beyond 2100, randomly chosen surface atmospheric forcings from 2091 to 2100 are used which means
311 that climate does not trend in time. RCP8.5 Projections beyond 2100 include significant continued warming
312 (Bulthuis and others, 2019) that we do not consider here and is an avenue for future research. There are no
313 forcing modifications made due to the evolution of the surface topography which means that as the WAIS
314 ice sheet surface lowers, there is no increase in surface melt from an increase in temperature expected due
315 to the atmospheric lapse rate. As such the so-called “surface-melt-elevation feedback” (e.g. Levermann and
316 Winkelmann, 2016) is absent from these simulations. This effect should be most significant where surface
317 temperatures rise above freezing in confined areas around the edges of the ice sheet that progress inward
318 as the WAIS collapses in the high-emissions scenarios.

319 Potentially countering this absent positive feedback for ice loss, is the increase in freezing precipitation
320 that should penetrate inwards as the WAIS melts. This is due to the reduction in blocking topography, the
321 penetration of open ocean inwards increasing surface fluxes that feed precipitating clouds, the temperature
322 increase allowing the air to hold more water, and the thickening troposphere with a greater precipitable
323 water content. These limitations in the method applied here may be less problematic if the ice melt is

324 strongly dominated by ocean melt, as has been proposed before (e.g. Pritchard and others, 2012).

325 Mass budgets are included in the Appendix and indicate that mass loss is dominated by basal melting
326 of floating ice. This highlights the importance of correctly simulating sub-ice-shelf melt given that the Ross
327 Ice Shelf undergoes collapse during phase 2 of our simulations.

328 The extended ABUMIP results produce a greater loss in ice mass than the extended ISMIP6 simulations.
329 This acts as a longer demonstration of the importance of the buttressing of ice shelves on AIS mass loss
330 already seen in ABUMIP (Sun and others, 2020). The negative feedback from bedrock rebound is revealed
331 by these experiments, with a reduction of about 1.5 m SLE by year 3000 attributable to it. This feedback
332 has been well documented in prior research (Gomez and others, 2010; Konrad and others, 2013; de Boer
333 and others, 2014; Gomez and others, 2015; Larour and others, 2019) and is proposed to work in a couple
334 of ways. As ice melts, the removal of ice mass causes the bedrock to rebound upwards creating a reduction
335 in slope from nearby still ice-covered regions towards the newly ice-free, or ice-reduced regions. A reduced
336 slope should tend to reduce ice sliding towards the ice-reduced regions. In addition, a grounding line with
337 a raised bedrock due to ice-mass loss will lower or eliminate sea water volume there, potentially reducing
338 the basal lubrication, which could act to reduce ice outflow. In addition to these effects, glacial isostatic
339 adjustment has a negative feedback on ice loss due to self gravitation effects from the lowering of relative
340 sea level as the ice sheet loses mass. This is not accounted for in these simulations and should act to
341 strengthen the negative feedback on ice loss.

342 The fact that we obtain a substantial retreat in the Wilkes Basin for the extreme ice shelf melt ex-
343 periments abum and abumiso, which does not occur in the float-kill experiments abuk and abukiso, is
344 counter-intuitive because float-kill should be the more extreme forcing (equivalent to infinite ice shelf
345 melt). The same behaviour was observed for some other models of the original ABUMIP exercise (Sun and
346 others, 2020). In case of SICOPOLIS, the reason is that the regional tuning of the basal sliding coefficient
347 produces a very low value for the Wilkes Basin (Greve and others, 2020, their Fig. 4). Our version of
348 the hybrid shallow-ice-shelfy-stream dynamics assumes that, below a slip ratio of 50%, pure shallow-ice
349 dynamics prevails. This is the case for almost the entire grounded region of the Wilkes Basin. Therefore,
350 in abuk and abukiso, the ice sheet does not experience a proper dynamic boundary condition at the marine
351 front (which exists only for shelfy-stream or shallow-shelf dynamics). Rather, at the front, the grounded ice
352 sees only the neighbouring grid points with zero thickness and zero velocity, which leads to an unphysical
353 blocking of the coastward ice flow. By contrast, in abum and abumiso, mini-ice shelves can survive despite

354 the large (but not infinite) melt rates. Therefore, the ice sheet experiences a proper boundary condition at
355 the calving front, which allows a realistic drainage of the ice, so that it thins and retreats more compared
356 to abuk and abukiso.

357 Changes to surface velocities due to bedrock rebound are dependent on the bed topography shape and
358 the distribution of the rebound. Predominantly, this effect acts to reduce surface velocities as described
359 above. However there are regions where bedrock rebound increases the slope towards the ocean and can
360 therefore act to increase ice sliding. For example on the northern coasts of the WAIS where ice remains,
361 regions of increased velocity can be seen in Figure 10. Therefore bedrock rebound causes a complicated
362 redistribution of ice producing regions of increased and decreased ice flow but dominated by the larger
363 areas where velocity decreases. These areas develop over the long term in the embayments large enough to
364 develop the relationship with rebound described above. Studies have found that the upper mantle under
365 the WAIS might be softer than elsewhere in Antarctica (van der Wal and others, 2015; Hay and others,
366 2017) and so might experience greater bedrock rebound. Therefore there is potential for these impacts on
367 the ice budget to be greater and more regionally dependent.

368 5 CONCLUSION

369 Ice-sheet simulations of extended versions of ISMIP6 future climate experiments for the AIS until the year
370 3000 have been analysed. The simulations use climate projections from the beginning of 2015 until the
371 end of 2100, after which no further climate trend is applied, with forcing selected randomly from the final
372 decade of the 21st century. For the unabated 21st century warming simulations, a large difference in the
373 vulnerability of East and West Antarctica develops over hundreds of years, with West Antarctica suffering
374 a much more severe ice loss than East Antarctica. In these cases, the mass loss amounts to an average
375 across the simulations of ~ 3.5 m SLE from 2015 to 3000. For the optimistic pathway, the mean mass loss is
376 ~ 0.24 m SLE. The results are radically different to the unclear response projected over the ISMIP6 period,
377 demonstrating that the consequences of the high-emissions scenario are much greater in the long term if a
378 sustained, late-21st-century climate is assumed.

379 Under the unabated 21st century warming scenario the ice sheet progresses through 4 phases, that are
380 defined by differing rates of ice loss. In our simulations these stages are attributable to how the WAIS loses
381 mass in the Ross Sea Embayment followed later by additional loss from the Amundsen Sea Embayment
382 and an eventual levelling-out in the rate of ice sheet loss once the majority of the WAIS has melted.

383 The ABUMIP experiments provide a demonstration of a bedrock rebound negative feedback that re-
384 duces ice loss in a similar manner as found in previous research. However bedrock rebound can lead to
385 faster ice flow in certain smaller areas where it acts to increase the slope towards the ocean. Limitations to
386 our study, pointing to possible directions for future work, include the lack of accounting for local climatic
387 changes in regions where ice-sheet collapse occurs causing a sharp drop in surface elevations with proba-
388 ble positive feedback from regional large surface temperature increases, and negative feedback from large
389 frozen precipitation increases.

390 SUPPLEMENTARY MATERIAL

391 Animations made using VAPOR (vapor.ucar.edu) using the NorESM forcing are included as supplementary
392 material. Frame interval is 20 years. In these the RCP2.6 projection is labelled as “Optimistic” and RCP8.5
393 is labelled as “Pessimistic”.

394 Animation NorESMrebound.mp4

395 RCP8.5 ice thickness (m) and bedrock rebound (m, colour scale in key).

396 Animation NorESMthick.mp4

397 RCP2.6 vs RCP8.5 comparison of ice thickness (m).

398 Animation NorESMthickchange.mp4

399 RCP2.6 vs RCP8.5 comparison of ice thickness difference from 2015 (m).

400 Animation NorESMvhs.mp4

401 RCP2.6 vs RCP8.5 comparison of surface ice velocity (m a^{-1}).

402 CODE AND DATA AVAILABILITY

403 SICOPOLIS is free and open-source software, available through a persistent Git repository hosted by the
404 Alfred Wegener Institute for Polar and Marine Research (AWI) in Bremerhaven, Germany (Greve and
405 SICOPOLIS Developer Team, 2021). Detailed instructions for obtaining and compiling the code are at
406 <http://www.sicopolis.net> (last access: 29 October 2021). The output data produced for this study are
407 available at Zenodo, <https://doi.org/10.5281/zenodo.5637797>.

408 ACKNOWLEDGEMENTS

409 We thank the two anonymous reviewers and the Scientific Editor Frank Pattyn for constructive remarks and
410 suggestions that helped to improve the manuscript. We thank the Climate and Cryosphere (CliC) effort,
411 which provided support for ISMIP6 through sponsoring of workshops, hosting the ISMIP6 website and
412 wiki, and promoting ISMIP6. We acknowledge the World Climate Research Programme, which, through
413 its Working Group on Coupled Modelling, coordinated and promoted CMIP5 and CMIP6. We thank the
414 climate modelling groups for producing their model output and making it available; the Earth System Grid
415 Federation (ESGF) for archiving the CMIP data and providing access to it; the University at Buffalo for
416 ISMIP6 data distribution and upload; and the multiple funding agencies who support CMIP5, CMIP6, and
417 ESGF. We thank the ISMIP6 steering committee, the ISMIP6 model selection group and ISMIP6 dataset
418 preparation group for their continuous engagement in defining ISMIP6. This is ISMIP6 contribution No.
419 25.

420 Christopher Chambers, Ralf Greve and Ayako Abe-Ouchi were supported by Japan Society for the
421 Promotion of Science (JSPS) KAKENHI Grant No. JP17H06323. Ralf Greve and Ayako Abe-Ouchi were
422 supported by JSPS KAKENHI Grant No. JP17H06104. Takashi Obase, Fuyuki Saito and Ayako Abe-Ouchi
423 were supported by JSPS Grant-in-Aid for Japan–France Integrated Action Program (SAKURA Program)
424 No. JPJSBP120213203.

425 REFERENCES

- 426 Alley RB, Anandakrishnan S, Christianson K, Horgan HJ, Muto A, Parizek BR, Pollard D and Walker RT (2015)
427 Oceanic forcing of ice-sheet retreat: West Antarctica and more. *Annual Review of Earth and Planetary Sciences*,
428 **43**(1), 207–231 (doi: 10.1146/annurev-earth-060614-105344)
- 429 Bamber JL, Riva REM, Vermeersen BLA and LeBrocq AM (2009) Reassessment of the potential sea-level rise from
430 a collapse of the West Antarctic Ice Sheet. *Science*, **324**(5929), 901–903 (doi: 10.1126/science.1169335)
- 431 Barthel A, Agosta C, Little CM, Hattermann T, Jourdain NC, Goelzer H, Nowicki S, Seroussi H, Straneo F and
432 Bracegirdle TJ (2020) CMIP5 model selection for ISMIP6 ice sheet model forcing: Greenland and Antarctica. *The
433 Cryosphere*, **14**(3), 855–879 (doi: 10.5194/tc-14-855-2020)
- 434 Bernales J, Rogozhina I, Greve R and Thomas M (2017) Comparison of hybrid schemes for the combination of
435 shallow approximations in numerical simulations of the Antarctic Ice Sheet. *The Cryosphere*, **11**(1), 247–265 (doi:
436 10.5194/tc-11-247-2017)

- 437 Bulthuis K, Arnst M, Sun S and Pattyn F (2019) Uncertainty quantification of the multi-centennial response of the
438 antarctic ice sheet to climate change. *The Cryosphere*, **13**(4), 1349–1380 (doi: 10.5194/tc-13-1349-2019)
- 439 Calov R, Beyer S, Greve R, Beckmann J, Willeit M, Kleiner T, Rückamp M, Humbert A and Ganopolski A (2018)
440 Simulation of the future sea level contribution of Greenland with a new glacial system model. *The Cryosphere*,
441 **12**(10), 3097–3121 (doi: 10.5194/tc-12-3097-2018)
- 442 de Boer B, Stocchi P and van de Wal RSW (2014) A fully coupled 3-D ice-sheet–sea-level model: algorithm and
443 applications. *Geoscientific Model Development*, **7**(5), 2141–2156 (doi: 10.5194/gmd-7-2141-2014)
- 444 Dutton A, Carlson AE, Long AJ, Milne GA, Clark PU, DeConto R, Horton BP, Rahmstorf S and Raymo ME
445 (2015) Sea-level rise due to polar ice-sheet mass loss during past warm periods. *Science*, **349**(6244), aaa4019 (doi:
446 10.1126/science.aaa4019)
- 447 Edwards TL, Nowicki S, Marzeion B, Hock R, Goelzer H, Seroussi H, Jourdain NC, Slater DA, Turner FE, Smith CJ,
448 McKenna CM, Simon E, Abe-Ouchi A, Gregory JM, Larour E, Lipscomb WH, Payne AJ, Shepherd A, Agosta C,
449 Alexander P, Albrecht T, Anderson B, Asay-Davis X, Aschwanden A, Barthel A, Bliss A, Calov R, Chambers C,
450 Champollion N, Choi Y, Cullather R, Cuzzzone J, Dumas C, Felikson D, Fettweis X, Fujita K, Galton-Fenzi BK,
451 Gladstone R, Golledge NR, Greve R, Hattermann T, Hoffman MJ, Humbert A, Huss M, Huybrechts P, Immerzeel
452 W, Kleiner T, Kraaijenbrink P, Le clec’h S, Lee V, Leguy GR, Little CM, Lowry DP, Malles JH, Martin DF,
453 Maussion F, Morlighem M, O’Neill JF, Nias I, Pattyn F, Pelle T, Price SF, Quiquet A, Radić V, Reese R, Rounce
454 DR, Rückamp M, Sakai A, Shafer C, Schlegel NJ, Shannon S, Smith RS, Straneo F, Sun S, Tarasov L, Trusel LD,
455 Van Breedam J, van de Wal R, van den Broeke M, Winkelmann R, Zekollari H, Zhao C, Zhang T and Zwinger
456 T (2021) Projected land ice contributions to twenty-first-century sea level rise. *Nature*, **593**(7857), 74–82 (doi:
457 10.1038/s41586-021-03302-y)
- 458 Eyring V, Bony S, Meehl GA, Senior CA, Stevens B, Stouffer RJ and Taylor KE (2016) Overview of the Coupled Model
459 Intercomparison Project Phase 6 (CMIP6) experimental design and organization. *Geoscientific Model Development*,
460 **9**(5), 1937–1958 (doi: 10.5194/gmd-9-1937-2016)
- 461 Fretwell P, Pritchard HD, Vaughan DG, Bamber JL, Barrand NE, Bell R, Bianchi C, Bingham RG, Blankenship DD,
462 Casassa G, Catania G, Callens D, Conway H, Cook AJ, Corr HFJ, Damaske D, Damm V, Ferraccioli F, Forsberg
463 R, Fujita S, Gim Y, Gogineni P, Griggs JA, Hindmarsh RCA, Holmlund P, Holt JW, Jacobel RW, Jenkins A,
464 Jokat W, Jordan T, King EC, Kohler J, Krabill W, Riger-Kusk M, Langley KA, Leitchenkov G, Leuschen C,
465 Luyendyk BP, Matsuoka K, Mouginot J, Nitsche FO, Nogi Y, Nost OA, Popov SV, Rignot E, Ripplin DM, Rivera
466 A, Roberts J, Ross N, Siegert MJ, Smith AM, Steinhage D, Studinger M, Sun B, Tinto BK, Welch BC, Wilson
467 D, Young DA, Xiangbin C and Zirizzotti A (2013) Bedmap2: improved ice bed, surface and thickness datasets for
468 Antarctica. *The Cryosphere*, **7**(1), 375–393 (doi: 10.5194/tc-7-375-2013)

- 469 Frieler K, Clark PU, He F, Buizert C, Reese R, Ligtenberg SRM, van den Broeke MR, Winkelmann R and Levermann
470 A (2015) Consistent evidence of increasing Antarctic accumulation with warming. *Nature Climate Change*, **5**(4),
471 348–352 (doi: 10.1038/nclimate2574)
- 472 Garbe J, Albrecht T, Levermann A, Donges JF and Winkelmann R (2020) The hysteresis of the Antarctic Ice Sheet.
473 *Nature*, **585**(7826), 538–544 (doi: 10.1038/s41586-020-2727-5)
- 474 Gasson E, DeConto RM, Pollard D and Levy RH (2016) Dynamic Antarctic ice sheet during the early to mid-Miocene.
475 *Proceedings of the National Academy of Sciences*, **113**(13), 3459–3464 (doi: 10.1073/pnas.1516130113)
- 476 Gladstone RM, Warner RC, Galton-Fenzi BK, Gagliardini O, Zwinger T and Greve R (2017) Marine ice sheet
477 model performance depends on basal sliding physics and sub-shelf melting. *The Cryosphere*, **11**(1), 319–329 (doi:
478 10.5194/tc-11-319-2017)
- 479 Golledge NR, Kowalewski DE, Naish TR, Levy RH, Fogwill CJ and Gasson EGW (2015) The multi-millennial
480 Antarctic commitment to future sea-level rise. *Nature*, **526**(7573), 421–425 (doi: 10.1038/nature15706)
- 481 Gomez N, Mitrovica JX, Huybers P and Clark PU (2010) Sea level as a stabilizing factor for marine-ice-sheet
482 grounding lines. *Nature Geoscience*, **3**(12), 850–853 (doi: 10.1038/ngeo1012)
- 483 Gomez N, Pollard D and Holland D (2015) Sea-level feedback lowers projections of future Antarctic Ice-Sheet mass
484 loss. *Nature Communications*, **6**(1), 8798 (doi: 10.1038/ncomms9798)
- 485 Greve R (1995) *Thermomechanisches Verhalten polythermer Eisschilde – Theorie, Analytik, Numerik*. Doctoral thesis,
486 Department of Mechanics, Darmstadt University of Technology, Germany (doi: 10.5281/zenodo.3815324)
- 487 Greve R (1997) Application of a polythermal three-dimensional ice sheet model to the Greenland ice sheet: Re-
488 sponse to steady-state and transient climate scenarios. *Journal of Climate*, **10**(5), 901–918 (doi: 10.1175/1520-
489 0442(1997)010<0901:AOAPTD>2.0.CO;2)
- 490 Greve R and SICOPOLIS Developer Team (2021) SICOPOLIS. GitLab, Alfred Wegener Institute for Polar and
491 Marine Research, Bremerhaven, Germany, URL <https://gitlab.awi.de/sicopolis/sicopolis>
- 492 Greve R, Calov R, Obase T, Saito F, Tsutaki S and Abe-Ouchi A (2020) ISMIP6 future projections for the Antarctic
493 ice sheet with the model SICOPOLIS. Technical report, Zenodo (doi: 10.5281/zenodo.3971232)
- 494 Hay CC, Lau HCP, Gomez N, Austermann J, Powell E, Mitrovica JX, Latychev K and Wiens DA (2017) Sea level
495 fingerprints in a region of complex earth structure: The case of wais. *Journal of Climate*, **30**(6), 1881 – 1892 (doi:
496 10.1175/JCLI-D-16-0388.1)

- 497 Joughin I and Alley RB (2011) Stability of the West Antarctic ice sheet in a warming world. *Nature Geoscience*,
498 4(8), 506–513 (doi: 10.1038/ngeo1194)
- 499 Joughin I, Smith BE and Medley B (2014) Marine ice sheet collapse potentially under way for the Thwaites Glacier
500 Basin, West Antarctica. *Science*, 344(6185), 735–738 (doi: 10.1126/science.1249055)
- 501 Jourdain NC, Asay-Davis X, Hattermann T, Straneo F, Seroussi H, Little CM and Nowicki S (2020) A protocol for
502 calculating basal melt rates in the ISMIP6 Antarctic ice sheet projections. *The Cryosphere*, 14(9), 3111–3134 (doi:
503 10.5194/tc-14-3111-2020)
- 504 Konrad H, Thoma M, Sasgen I, Klemann V, Grosfeld K, Barbi D and Martinec Z (2013) The deformational response
505 of a viscoelastic solid earth model coupled to a thermomechanical ice sheet model. *Surveys in Geophysics* (doi:
506 10.1007/s10712-013-9257-8)
- 507 Krinner G, Magand O, Simmonds I, Genthon C and Dufresne JL (2007) Simulated Antarctic precipitation and
508 surface mass balance at the end of the twentieth and twenty-first centuries. *Climate Dynamics*, 28(2-3), 215–230
509 (doi: 10.1007/s00382-006-0177-x)
- 510 Larour E, Seroussi H, Adhikari S, Ivins E, Caron L, Morlighem M and Schlegel N (2019) Slowdown in antarctic mass
511 loss from solid earth and sea-level feedbacks. *science*, 364(6444) (doi: 10.1126/science.aav7908)
- 512 Levermann A and Winkelmann R (2016) A simple equation for the melt elevation feedback of ice sheets. *The*
513 *Cryosphere*, 10(4), 1799–1807 (doi: 10.5194/tc-10-1799-2016)
- 514 Levermann A, Clark PU, Marzeion B, Milne GA, Pollard D, Radic V and Robinson A (2013) The multimillennial
515 sea-level commitment of global warming. *Proceedings of the National Academy of Sciences*, 110(34), 13745–13750
516 (doi: 10.1073/pnas.1219414110)
- 517 Ligtenberg SRM, van de Berg WJ, van den Broeke MR, Rae JGL and van Meijgaard E (2013) Future surface mass
518 balance of the Antarctic ice sheet and its influence on sea level change, simulated by a regional atmospheric climate
519 model. *Climate Dynamics*, 41(3-4), 867–884 (doi: 10.1007/s00382-013-1749-1)
- 520 Lipscomb WH, Leguy GR, Jourdain NC, Asay-Davis X, Seroussi H and Nowicki S (2021) ISMIP6-based projections of
521 ocean-forced Antarctic Ice Sheet evolution using the Community Ice Sheet Model. *The Cryosphere*, 15(2), 633–661
522 (doi: 10.5194/tc-15-633-2021)
- 523 Mercer JH (1968) Antarctic ice and Sangamon sea level. In *Bern General Assembly, Commission of Snow and Ice*,
524 1967, IAHS Publication No. 79, 217–225, International Association of Hydrological Sciences
- 525 Nowicki S, Goelzer H, Seroussi H, Payne AJ, Lipscomb WH, Abe-Ouchi A, Agosta C, Alexander P, Asay-Davis
526 XS, Barthel A, Bracegirdle TJ, Cullather R, Felikson D, Fettweis X, Gregory JM, Hattermann T, Jourdain NC,

- 527 Kuipers Munneke P, Larour E, Little CM, Morlighem M, Nias I, Shepherd A, Simon E, Slater D, Smith RS, Straneo
528 F, Trusel LD, van den Broeke MR and van de Wal R (2020) Experimental protocol for sea level projections from
529 ISMIP6 stand-alone ice sheet models. *The Cryosphere*, **14**(7), 2331–2368 (doi: 10.5194/tc-14-2331-2020)
- 530 Nowicki SMJ, Payne A, Larour E, Seroussi H, Goelzer H, Lipscomb W, Gregory J, Abe-Ouchi A and Shepherd A
531 (2016) Ice Sheet Model Intercomparison Project (ISMIP6) contribution to CMIP6. *Geoscientific Model Develop-*
532 *ment*, **9**(12), 4521–4545 (doi: 10.5194/gmd-9-4521-2016)
- 533 Payne AJ, Nowicki S, Abe-Ouchi A, Agosta C, Alexander P, Albrecht T, Asay-Davis X, Aschwanden A, Barthel
534 A, Bracegirdle TJ, Calov R, Chambers C, Choi Y, Cullather R, Cuzzone J, Dumas C, Edwards TL, Felikson
535 D, Fettweis X, Galton-Fenzi BK, Goelzer H, Gladstone R, Golledge NR, Gregory JM, Greve R, Hattermann T,
536 Hoffman MJ, Humbert A, Huybrechts P, Jourdain NC, Kleiner T, Munneke PK, Larour E, Le clec'h S, Lee V,
537 Leguy G, Lipscomb WH, Little CM, Lowry DP, Morlighem M, Nias I, Pattyn F, Pelle T, Price SF, Quiquet A,
538 Reese R, Rückamp M, Schlegel NJ, Seroussi H, Shepherd A, Simon E, Slater D, Smith RS, Straneo F, Sun S,
539 Tarasov L, Trusel LD, Van Breedam J, van de Wal R, van den Broeke M, Winkelmann R, Zhao C, Zhang T and
540 Zwinger T (2021) Future sea level change under CMIP5 and CMIP6 scenarios from the Greenland and Antarctic
541 ice sheets. *Geophysical Research Letters* (doi: 10.1029/2020GL091741), in press
- 542 Pollard D and DeConto RM (2009) Modelling West Antarctic ice sheet growth and collapse through the past five
543 million years. *Nature*, **458**(7236), 329–332 (doi: 10.1038/nature07809)
- 544 Pritchard HD, Ligtenberg SRM, Fricker HA, Vaughan DG, van den Broeke MR and Padman L (2012) Antarctic
545 ice-sheet loss driven by basal melting of ice shelves. *Nature*, **484**(7395), 502–505 (doi: 10.1038/nature10968)
- 546 Rignot E and Mouginot J (2016) Antarctica and Greenland drainage basin and ice sheet definitions. IMBIE 2016
- 547 Rignot E, Mouginot J, Morlighem M, Seroussi H and Scheuchl B (2014) Widespread, rapid grounding line retreat
548 of Pine Island, Thwaites, Smith, and Kohler glaciers, West Antarctica, from 1992 to 2011. *Geophysical Research*
549 *Letters*, **41**(10), 3502–3509 (doi: 10.1002/2014GL060140)
- 550 Sato T and Greve R (2012) Sensitivity experiments for the Antarctic ice sheet with varied sub-ice-shelf melting rates.
551 *Annals of Glaciology*, **53**(60), 221–228 (doi: 10.3189/2012AoG60A042)
- 552 Schaeffer M, Hare W, Rahmstorf S and Vermeer M (2012) Long-term sea-level rise implied by 1.5 °C and 2 °C
553 warming levels. *Nature Climate Change*, **2**(12), 867–870 (doi: 10.1038/nclimate1584)
- 554 Schoof C (2007) Ice sheet grounding line dynamics: Steady states, stability, and hysteresis. *Journal of Geophysical*
555 *Research: Earth Surface*, **112**(F3), F03S28 (doi: 10.1029/2006JF000664)

- 556 Seroussi H, Nowicki S, Payne AJ, Goelzer H, Lipscomb WH, Abe-Ouchi A, Agosta C, Albrecht T, Asay-Davis X,
557 Barthel A, Calov R, Cullather R, Dumas C, Galton-Fenzi BK, Gladstone R, Golledge N, Gregory JM, Greve R,
558 Hatterman T, Hoffman MJ, Humbert A, Huybrechts P, Jourdain NC, Kleiner T, Larour E, Leguy GR, Lowry DP,
559 Little CM, Morlighem M, Pattyn F, Pelle T, Price SF, Quiquet A, Reese R, Schlegel NJ, Shepherd A, Simon E,
560 Smith RS, Straneo F, Sun S, Trusel LD, Van Breedam J, van de Wal RSW, Winkelmann R, Zhao C, Zhang T and
561 Zwinger T (2020) ISMIP6 Antarctica: a multi-model ensemble of the Antarctic ice sheet evolution over the 21st
562 century. *The Cryosphere*, **14**(9), 3033–3070 (doi: 10.5194/tc-14-3033-2020)
- 563 Sun S, Pattyn F, Simon EG, Albrecht T, Cornford S, Calov R, Dumas C, Gillet-Chaulet F, Goelzer H, Golledge NR,
564 Greve R, Hoffman MJ, Humbert A, Kazmierczak E, Kleiner T, Leguy GR, Lipscomb WH, Martin D, Morlighem
565 M, Nowicki S, Pollard D, Price S, Quiquet A, Seroussi H, Schlemm T, Sutter J, van de Wal RSW, Winkelmann R
566 and Zhang T (2020) Antarctic ice sheet response to sudden and sustained ice-shelf collapse (ABUMIP). *Journal*
567 *of Glaciology*, **66**(260), 891–904 (doi: 10.1017/jog.2020.67)
- 568 The IMBIE team (2018) Mass balance of the Antarctic Ice Sheet from 1992 to 2017. *Nature*, **558**(7709), 219–222
569 (doi: 10.1038/s41586-018-0179-y)
- 570 Trusel LD, Frey KE, Das SB, Karnauskas KB, Kuipers Munneke P, van Meijgaard E and van den Broeke MR
571 (2015) Divergent trajectories of Antarctic surface melt under two twenty-first-century climate scenarios. *Nature*
572 *Geoscience*, **8**(12), 927–932 (doi: 10.1038/ngeo2563)
- 573 Turney CSM, Fogwill CJ, Golledge NR, McKay NP, van Sebille E, Jones RT, Etheridge D, Rubino M, Thornton DP,
574 Davies SM, Ramsey CB, Thomas ZA, Bird MI, Munksgaard NC, Kohno M, Woodward J, Winter K, Weyrich LS,
575 Rootes CM, Millman H, Albert PG, Rivera A, van Ommen T, Curran M, Moy A, Rahmstorf S, Kawamura K,
576 Hillenbrand CD, Weber ME, Manning CJ, Young J and Cooper A (2020) Early Last Interglacial ocean warming
577 drove substantial ice mass loss from Antarctica. *Proceedings of the National Academy of Sciences*, **117**(8), 3996–
578 4006 (doi: 10.1073/pnas.1902469117)
- 579 Uotila P, Lynch AH, Cassano JJ and Cullather RI (2007) Changes in Antarctic net precipitation in the 21st century
580 based on Intergovernmental Panel on Climate Change (IPCC) model scenarios. *Journal of Geophysical Research:*
581 *Atmospheres*, **112**(D10), D10107 (doi: 10.1029/2006JD007482)
- 582 van der Wal W, Whitehouse PL and Schrama EJ (2015) Effect of GIA models with 3D composite mantle viscosity
583 on GRACE mass balance estimates for Antarctica. *Earth and Planetary Science Letters*, **414**, 134–143 (doi:
584 10.1016/j.epsl.2015.01.001)

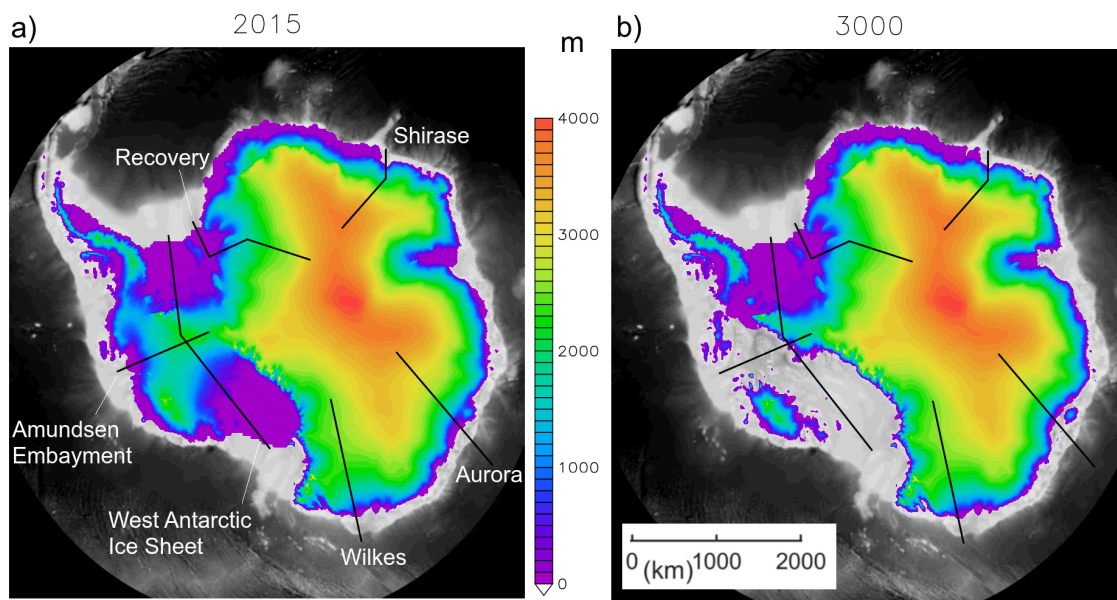


Fig. 12. Cross-section locations on surface topography for the MIROC-ESM-CHEM RCP8.5 experiment for a) 2015, and b) 3000. Included are cross-section locations for the WAIS used in Figure 4 and the Amundsen Embayment in Figure 6.

585 A APPENDIX

586 This appendix presents additional cross-sections and mass budgets for the MIROC-ESM-CHEM RCP8.5
 587 case. Considered first are four EAIS cross-sections, guided by the ice flow line, for the Recovery, Shirase,
 588 Aurora, and Wilkes basins. The locations of the cross-sections, as well as those shown earlier in Figures 4
 589 and 6, are in Figure 12. The cross-sections shown in Figure 13 all show far less change than those for the
 590 WAIS. In the extreme, the Shirase section shows so little ice change at the coast that all profiles from 2015
 591 to 3000 appear to overlap to form one line. The only change in this profile is from the slow thickening of
 592 the interior ice. The Recovery and Wilkes cross-sections show some minor ice shelf basal melt, however
 593 there again is essentially no coastal retreat. Of the four, the Aurora basin has the greatest response
 594 with ~ 150 km retreat in the ice at the coast. The loss in coastal ice, combined with the thickening of
 595 interior ice, steepens the ice sheet slopes slightly, with the greatest steepening in the Aurora basin. Further
 596 investigation is recommended to determine why so little simulated change is seen in East Antarctica.

597 Secondly, mass budgets are shown in Figure 14. The mass loss is driven almost entirely by basal mass
 598 loss from floating ice. Comparing the regionally divided figures indicates that the rapid ice loss during
 599 phase 3 is driven primarily by basal mass loss from floating ice in the WAIS. The sharp dip in the rate of

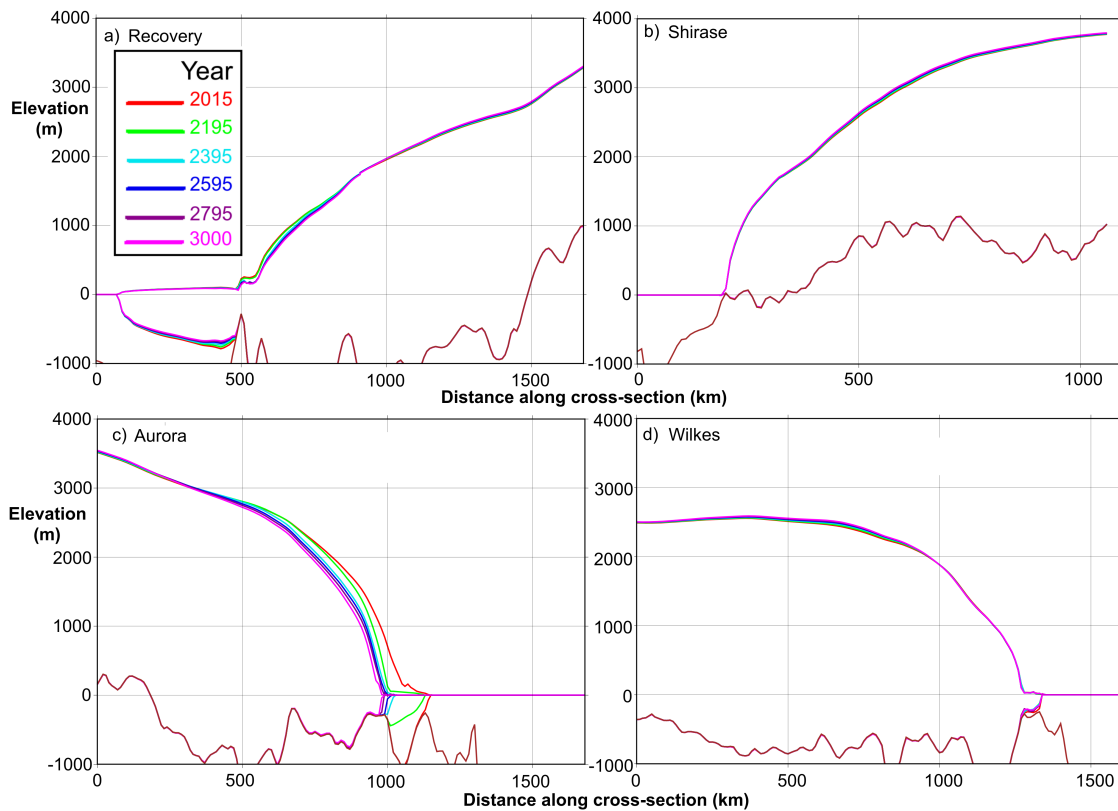


Fig. 13. EAIS ice profile cross-sections for a) Recovery, b) Shirase, c) Aurora, and d) Wilkes for the years indicated.

600 volume change around 2100 is associated with the transition from a warming climate to a constant climate.
601 The total surface mass balance declines between 2100 and 3000 over the WAIS. This may be due to the
602 reduction in surface ice area or the redistribution of ice away from areas of positive mass balance in the
603 end of 21st century forcing data used.

For Peer Review

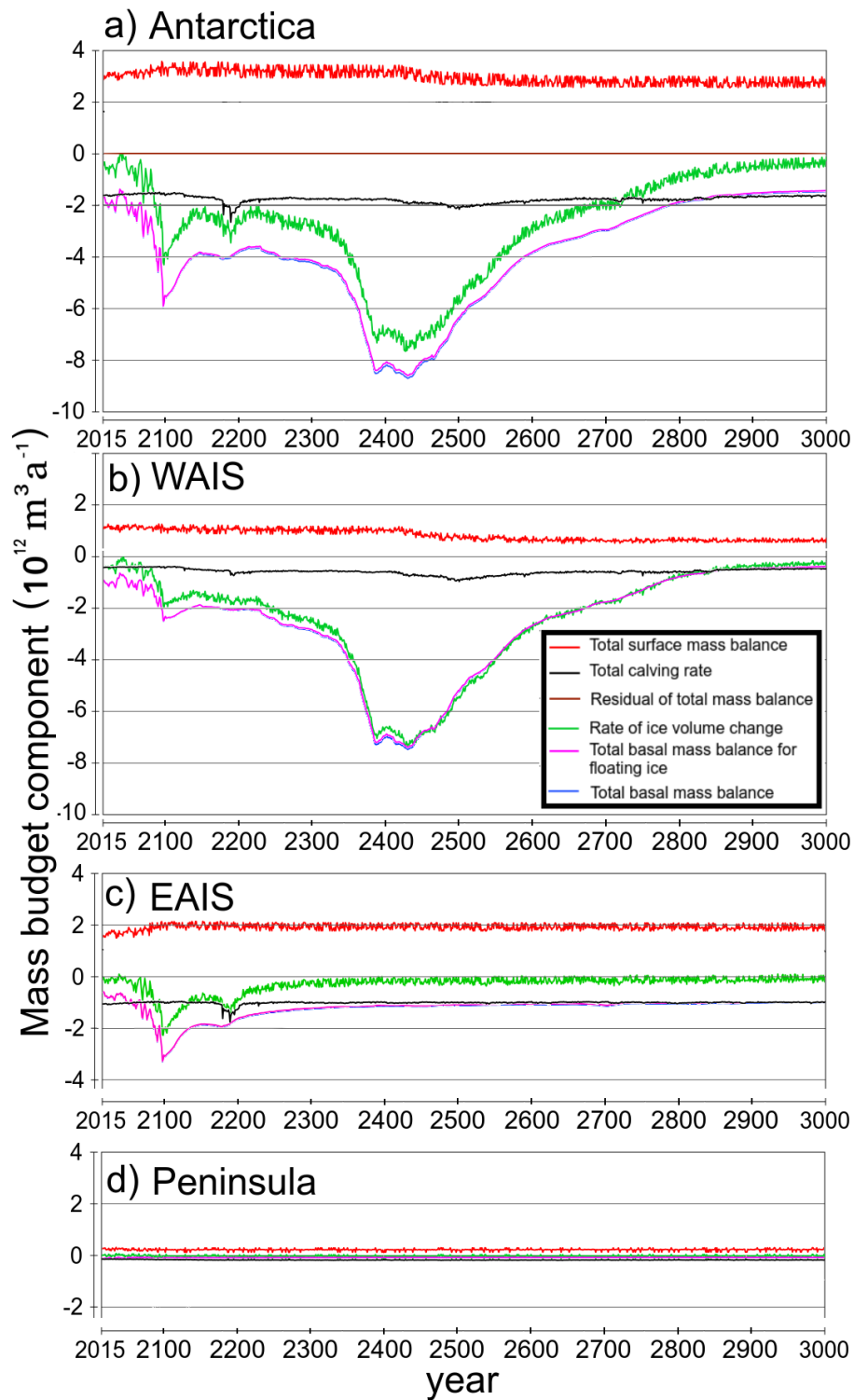


Fig. 14. Mass budget components for the MIROC-ESM-CHEM RCP8.5 case for a) all Antarctica, b) WAIS, c) EAIS, and d) the Antarctic Peninsula.